energy&fuels

pubs.acs.org/EF

Article

Sustainable Resource Recovery from Dairy Waste: A Case Study of Hydrothermal Co-liquefaction of Acid Whey and Anaerobic Digestate Mixture

Hanifrahmawan Sudibyo* and Jefferson William Tester

Cite This: https://doi.org/10.1021/acs.energyfuels.2c03860

Read Online

ACCESS | Metrics & More | Article Recommendations | Supporting Information

ABSTRACT: Uncontrolled emission of carbon and nutrients due to mismanagement of dairy waste leads to global warming, eutrophication of water bodies, aerosol pollution, and acidification of ecosystems. We studied hydrothermal liquefaction (HTL) to sustainably recover resources by converting the dairy wastes into carbon-dense biocrude oil and a nutrient-rich aqueous-phase coproduct. We evaluated acid whey as an alternative source of acid catalyst, replacing acetic acid, for the HTL of anaerobically digested cattle manure (manure digestate). Using well-designed HTL experiments, we investigated the effects of several factors on the product formation and the fate of elements as well as the underlying chemistry. The investigated factors included reaction temperature (280−360 °C), reaction time (10−50 min), mixing ratio of acid whey to manure digestate (AW/MD of 0−2), and the amount of additional acetic acid required, that is, specified based on the final feedstock pH between 3.5 and 5.5. The experimental results suggested the following optimal conditions for enhanced biocrude oil formation and maximal nutrient yield in the aqueous-phase coproduct: AW/MD of 1.21, feedstock mixture pH of 4.5, and reaction temperature and time of 354 °C and 21 min, respectively. Under such conditions, the biocrude oil yield was enhanced to 40−50% (equivalent to 60−80% energy recovery) via cyclic acetalization, hydroxymethylation, isomerization, Piancatelli rearrangement, oxidation, and condensation with heteroatom removal via several deoxygenation and denitrogenation mechanisms. Moreover, these conditions provided adequate acidification to solubilize Mg-carbonate and Ca-phosphate minerals and catalyzed the deamination of N-heterocyclics and other nitrogenous compounds, producing a higher recoverable yield of Mg, NH_3-N, P, and K nutrients in the aqueous-phase coproduct, that is, 60−70, 30−40, ∼40, and >95%, respectively. This study demonstrated the potential of using HTL for coprocessing manure digestate and acid whey to measurably valorize biomass waste as a key component of achieving a circular bioeconomy for the dairy industry.

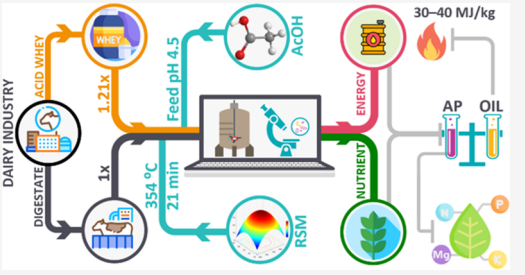

1. INTRODUCTION

Acid whey (i.e., a lactose-rich liquid leftover from the production of Greek yogurt and acid-coagulated cheeses) and manure digestate (i.e., a lignocellulose- and nutrient-rich wet residue from anaerobic digestion of cattle manure) are two primary byproducts from the dairy industry that could be coprocessed as feedstocks to recover energy, nutrients, and other coproducts. Approximately, 10 million metric tons of acid whey (AW) is generated annually from the Greek yogurt and acid-coagulated cheese production facilities in the United States.[1] In addition, an estimated 2.7 billion tons of manure digestate (MD) is produced each year by anaerobically digesting the manure generated by 94 million cattle housed in 883,000 concentrated animal feeding operations (CAFOs) in the United States.[2] This estimate of manure digestate assumes that all CAFOs in the United States use anaerobic digestion as a first step for treating the manure. In the anaerobic digestion, the average amount of dry matter in manure is 10%,[3] and the average removal of the volatile solid (i.e., organic substances that can be (bio)chemically transformed into gas) after anaerobic digestion is 60%.[4,5] Effective treatment of these mixed feedstocks requires careful attention to the locations and sizes of CAFOs and yogurt production facilities as well as the physicochemical properties of the waste streams. Despite their different pH values, manure digestate (pH 7−9) and acid whey (pH 3−5.5) generally share relatively similar properties including high moisture content (between 85 and 95 wt %),[6,7] high chemical oxygen demand (between 50 and 120 mg/g),[8,9] and high nutrient concentration, for example, 1500−6800 ppm NH_3-N, 150−620 ppm P, and 1200−9700 ppm K.[10,11] With these characteristics, mismanagement of these byproducts may result in several impacts that are detrimental to the environment, such as the production of methane and other greenhouse gases, the spread of pathogens, eutrophication of water basins, and acidification of ecosystems

Received: November 14, 2022
Revised: January 15, 2023

due to nutrient runoff, phytotoxicity, and the formation and release of ammonium aerosol salts causing aerosol pollution.[10,12−14]

The development of waste management strategies focusing on sustainable resource recovery within the circular bioeconomy (CBE) framework offers a means to mitigate these potential environmental threats while providing economic benefits to the dairy industry.[15,16] The resource recovery in the CBE framework is achieved by employing a combination of several unit processes to valorize biomass waste via multiple conversion pathways into valuable products in line with the bio-based economy's value pyramid (i.e., pharmaceuticals and fine chemicals, food and feed, functional and commodity chemicals, and energy, heat, and fuel) and waste hierarchy, that is, prevention, reuse, recycling, recovery, and disposal.[17]

Hydrothermal liquefaction (HTL) is an attractive thermochemical waste reforming process that can be incorporated into CBE systems due to its capability of handling the high moisture content of different types of agricultural and food wastes.[18,19] This includes anaerobic digestate produced by anaerobic digestion (AD), allowing HTL to be coupled with the commercially available AD process.[20] HTL benefits from the change of water properties at near-supercritical conditions (280−360 °C and 10−20 MPa), where the ionic product of water increases from 10−14 at 25 °C to 10−12 and 10−11 at 280−360 °C and the dielectric constant of water decreases from 80 at 25 °C to 15 at 360 °C.[18] With these properties, HTL can convert the organic matrix in high-moisture dairy wastes into carbon-rich biocrude oil with low heteroatom content and improved energy recovery and selectively extracts the inorganic nutrients into the aqueous-phase coproduct (HTL-AP) or precipitate them into the solid byproduct called hydro-char.[21,22] The near-supercritical water temperature of HTL can also kill pathogens in the dairy waste, yielding a sterilized effluent.[23]

Achieving both high energy recovery in biocrude oil and significant nutrient recovery in HTL coproducts depends on the thermodynamic and chemical changes occurring during the conversion process, which are controlled by operating conditions and feedstock properties. An earlier study[24] on the HTL of manure digestate with various salt compositions and polysaccharide-to-lignin ratios reported the significance of acidic pH (3.0−5.6) for the feedstock, in addition to the optimized reaction temperatures (335−360 °C), operating pressures (10−20 MPa), and reaction times (10−50 min), to achieve both waste treatment goals. These optimal conditions allowed to recover 58−75% of the carbon in biocrude oil, minimize the oxygen (15−35%) and nitrogen (0.2−1.5%) contents of biocrude oil, lower the yield of undesirable hydrochar byproduct to as low as 5 to 16%, and maximize the distribution of Mg (60−85%), Ca (33−46%), NH_3-N (41−52%), P (41−74%), and K (89−96%) in the HTL-AP. Given that the pre-acidification step increases the operational cost of HTL of manure digestates,[25,26] alternative strategies such as HTL coprocessing (co-liquefaction) with acidic feedstocks that can be collected from the same industry sector such as acid whey[27] are worth investigating.

One benefit of co-liquefaction of an acid whey−manure digestate mixture is that acid whey itself may partially or completely supply the acidity needed to catalyze the biocrude oil-forming and nutrient solubilization reactions. The main sources of acidity in acid whey are lactic acid, which is a byproduct of milk fermentation into soft cheese and Greek yogurt and acidic phosphate salts (KH_2PO_4 and NaH_2PO_4), which are additives in milk to maintain milk protein stability. Another benefit is that the acids contained in acid whey may facilitate reductive depolymerization of lignin and hydroxymethylation, cyclic acetalization, and pyran formation of lignin-derived oily monomers, enhancing lignin conversion into biocrude oil.[28] These acids may also solubilize mineral nutrients in the digestate, resulting in higher nutrient yield in HTL-AP and ultimately allowing post-HTL nutrient recovery via struvite ($MgNH_4PO_4{\cdot}6H_2O$) crystallization,[29] ammonia air stripping,[30] and membrane separation.[31] Moreover, the mixing of acid whey and digestates increases the polysaccharide-to-lignin ratio in the HTL feedstock because of high lactose content in acid whey. The HTL of feedstocks with higher polysaccharide-to-lignin ratios has been reported to give higher biocrude oil yield.[24]

An earlier study on HTL of acid whey[32] demonstrated that an alkaline feedstock pH is favored to (1) maximize biocrude oil yield with high carbon content and low heteroatom content, (2) minimize the formation of hydro-char and, therefore, higher nutrient yield in HTL-AP, and (3) produce aqueous organics that catalyze the deamination of amino acids into aqueous-phase NH_3-N. The co-liquefaction of acidic mixtures of acid whey and manure digestate by HTL has not been examined and may be able to produce comparable or better results as well as improve the overall economics of dairy waste management. Therefore, this study aims to (1) understand how coprocessing acid whey and manure digestate with different mixing ratios at various co-liquefaction operating conditions affects the product distribution and the fate of elements; (2) determine if adding organic acid catalysts, such as acetic acid, is still needed after mixing manure digestate with acid whey; and (3) determine optimum co-liquefaction operating conditions that maximize energy recovery in biocrude oil and nutrient yield in HTL-AP.

To achieve these objectives, we created an experimental program following central composite design protocols. Three factors were selected as the continuous independent variables: reaction temperature, reaction time, and mixing ratio between acid whey and manure digestate (AW/MD). Various response variables were measured to perform regression analysis and response surface optimization. The regression analysis provides a measure of the statistical significance of the investigated independent variables. The response surface optimization employing the desirability function approach was performed to specify a range of optimal HTL operating conditions for various acid whey and manure digestate mixing ratios that yielded maximal biocrude energy recovery (i.e., a high oil yield with a high carbon content and low heteroatom content), low hydro-char yield, and maximal Mg, NH_3-N, and P yields and minimal Ca yield in HTL-AP; these latter yields are attractive for the nutrient recovery process, for example, struvite production and membrane separation.[33,34] The minimal Ca distribution into the HTL-AP allows for higher struvite purity and prevents membrane fouling for an extended lifetime. The optimized reaction temperature and time were validated through additional triplicated HTL experiments (herein referred to as "validation experiment") on feedstock with different mixture compositions. A combination of reaction temperature, reaction time, and AW/MD mixing ratio that produced these optimal results was subsequently employed in the triplicated HTL "evaluation experiments". In these experiments, the mixture of manure digestate and acid whey

https://doi.org/10.1021/acs.energyfuels.2c03860
Energy Fuels XXXX, XXX, XXX−XXX

was acidified with different amounts of acetic acid. Results of these experiments allowed us to determine how much acetic acid was needed to convert the mixed feedstocks into desired products with specific characteristics.

2. MATERIALS AND METHODS

2.1. Feedstocks and Reagents. Co-liquefaction feedstocks were a mixture of raw acid whey and anaerobic digestate of cattle manure (herein referred to as "manure digestate"). Raw acid whey was taken from FAGE USA Dairy Industry Inc. (Johnstown, NY), and manure digestate was collected from Sunnyside dairy farm (Scipio Center, NY). Their physicochemical characteristics are given in Table 1.

Table 1. Physicochemical Characteristics of Raw Acid Whey and Manure Digestate[a]

parameters	value	
	acid whey	manure digestate
pH	4.38 ± 0.22	7.26 ± 0.35
NH_3-N(mg/L)	96 ± 4.41	3396 ± 7.50
DM (% FM)	5.14 ± 0.86	14.87 ± 0.50
ash content (% DM)	19.91 ± 1.21	26.81 ± 2.45
proximate analysis (% DM)		
cellulose		17.88 ± 0.76
hemicellulose		8.95 ± 1.05
soluble sugars	66.86 ± 0.38	
lignin		27.24 ± 3.95
lipid	1.36 ± 0.57	0.96 ± 0.37
protein	9.55 ± 1.14	7.69 ± 0.84
organic acids	2.63 ± 0.26	0.64 ± 0.15
ultimate analysis (% DM)		
C	36.96 ± 3.31	33.96 ± 2.96
H	5.78 ± 0.28	4.68 ± 0.39
N	1.01 ± 0.29	3.16 ± 0.61
O	48.16 ± 1.69	43.42 ± 0.64
P	1.05 ± 0.37	1.21 ± 0.40
K	2.53 ± 0.78	4.57 ± 0.67
Ca	2.33 ± 1.17	3.09 ± 0.34
Mg	0.12 ± 0.04	2.15 ± 0.81
Cl	4.11 ± 0.43	1.25 ± 0.16

[a]Analytical procedures are summarized in Table S1 in the Supporting Information (DM = dry matter and FM = fresh matter).

Organic solvents for biocrude oil extraction were acetone, dichloromethane, and ethyl acetate in ACS grade (Fisher Chemical). Anhydrous $MgSO_4$ (Santa Cruz Biotechnology) was used to remove residual water in the biocrude oil−solvent mixtures before solvent evaporation. Acetic acid glacial (Fisher Chemical) were used to adjust the feedstock pH. Reagents for colorimetric analysis were purchased from Hanna Instruments.

2.2. HTL Procedures and Product Characterization. The experimental setup and procedures were similar to those described in our previous study (see Figure S1 in the Supporting Information).[35] From each set of experiment, the collected products were (1) biocrude oil, a mixture of three biocrude extraction fractions, that is, dichloromethane- and ethyl-acetate-extracted water-soluble biocrudes and dichloromethane-extracted solid-bound biocrude; (2) solid byproduct, that is, hydro-char; and (3) aqueous-phase coproduct (HTL-AP). The mass yield of biocrude oil or hydro-char was calculated using eq 1.

$$Y_i = \frac{m_i}{m_{\text{feedstock}}} \times 100\% \quad (1)$$

where Y is the mass yield, i indicates biocrude oil or hydro-char, m is mass (g), and $m_{\text{feedstock}}$ is the dry mass of feedstock (g).

The yield of carbon or nitrogen in the biocrude oil or hydro-char and in the HTL-AP was calculated using eqs 2−4, respectively.

$$X_{\text{yield-i}} = \frac{(\%\, X_i) \times m_i}{X_{\text{feedstock}}} \times 100\% \quad (2)$$

$$C_{\text{yield-AP}} = \frac{[\text{TOC}]_{\text{AP}} \times (V_{\text{AP}})}{X_{\text{feedstock}}} \times 100\% \quad (3)$$

$$N_{\text{yield-AP}} = \frac{[\text{TN}]_{\text{AP}} \times (V_{\text{AP}})}{X_{\text{feedstock}}} \times 100\% \quad (4)$$

where $X_{\text{feedstock}}$ and X_{yield} represent the elemental mass in the feedstock (g) and elemental yield of carbon or nitrogen, respectively; i indicates biocrude oil or hydro-char; and % X is the carbon or nitrogen content measured following the ASTM D5373-21 method[36] (Exeter Analytical CE-440 CHN/O Analyzer). $C_{\text{yield-AP}}$ and $N_{\text{yield-AP}}$ are the carbon and nitrogen yield, respectively, in the HTL-AP, and $[\text{TOC}]_{\text{AP}}$ and $[\text{TN}]_{\text{AP}}$ are the total concentration of organic carbon and nitrogen (mg/L), respectively. The $[\text{TOC}]_{\text{AP}}$ and $[\text{TN}]_{\text{AP}}$ measurements follow the catalytic oxidation method at 720 °C using integrated Shimadzu TOC-L and TNM-L modules.

The yields of carbon and nitrogen expelled to the gas phase ($C_{\text{yield-gas}}$ and $N_{\text{yield-gas}}$) during reaction were estimated by difference using the calculated yields of carbon and nitrogen in the biocrude oil, hydro-char, and HTL-AP (eqs 5 and 6). The reproducibility of this approach is verified by the low standard deviation of $C_{\text{yield-gas}}$ and $N_{\text{yield-gas}}$ (see Tables S8−S9 in the Supporting Information). Afterward, the gas yield (Y_{gas}) was calculated according to $C_{\text{yield-gas}}$ using eq 7 by assuming that the gas comprised mostly CO_2. The mass yield of HTL-AP (Y_{AP}) was estimated using eq 8.

$$C_{\text{yield-gas}} = 100\% - C_{\text{yield-biocrude}} - C_{\text{yield-HC}} - C_{\text{yield-AP}} \quad (5)$$

$$N_{\text{yield-gas}} = 100\% - N_{\text{yield-biocrude}} - N_{\text{yield-HC}} - N_{\text{yield-AP}} \quad (6)$$

$$Y_{\text{gas}} = \frac{44}{12} \times \frac{C_{\text{yield-gas}} \times C_{\text{feedstock}}}{m_{\text{feedstock}}} \times 100\% \quad (7)$$

$$Y_{\text{AP}} = 100\% - Y_{\text{biocrude}} - Y_{\text{HC}} - Y_{\text{gas}} \quad (8)$$

The yields of nutrient (Z—P, Ca, Mg, K, or Cl) in hydro-char (Z_{HC}) and HTL-AP (Z_{AP}) were calculated using eqs 9 and 10, respectively.

$$Z_{\text{HC}} = \frac{\%\, Z_{\text{HC}} \times m_{\text{HC}}}{Z_{\text{feedstock}}} \times 100\% \quad (9)$$

$$Z_{\text{AP}} = \frac{[Z]_{\text{AP}} \times V_{\text{AP}}}{Z_{\text{feedstock}}} \times 100\% \quad (10)$$

where $Z_{\text{feedstock}}$ is the mass of Z in the feedstock (g), V_{AP} is the HTL-AP volume, and m_{HC} is the hydro-char mass (g). % Z_{HC} is the elemental content in hydro-char measured using an Oxford Instruments EDX spectrometer (with AZtecLive and Ultim Max detector) integrated with a Zeiss Gemini 500 scanning electron microscope. The SEM−EDX operating parameters are as follows: 20 keV electron beam, 8 mm working distance, 60 μm lens aperture size, InLens detector, 1024 pixels resolution, 6 s process time, and 120 s acquisition time. $[Z]_{\text{AP}}$ is the colorimetrically measured nutrient concentration (mg/L) using a Hanna Instrument HI83399 photometer. The aqueous concentrations of NH_3-N, P, K, Ca, and Mg were determined with ASTM D1426-15,[37] vanadomolybdophosphoric acid,[38] sodium tetraphenylborate,[39] oxalate,[40] and Calmagite[41] methods, respectively.

The biocrude energy recovery (ER_{Oil}) was calculated using eq 11, with the higher heating value of dry co-liquefaction feedstock ($HHV_{\text{feedstock}}$, MJ/kg) and biocrude oil (HHV_{oil}, MJ/kg) estimated using the equation by Channiwala and Parikh[42] based on the measured C, H, N, O, and ash contents. The ash content was determined with the ASTM E1131-20 method.[43]

https://doi.org/10.1021/acs.energyfuels.2c03860
Energy Fuels XXXX, XXX, XXX−XXX

$$ER_{oil} = \frac{HHV_{oil}}{HHV_{feedstock}} \times Y_{oil} \times 100\% \quad (11)$$

The GC−MS compositional analysis was performed on selected biocrude oil and HTL-AP samples using Agilent 6890N GC equipped with a JEOL JMS-GCMATE II mass spectrometer. The GC−MS operating procedures employing DB-5 and DB-WAX UI columns for biocrude oil and HTL-AP samples, respectively, are given in Tables S2 and S3. The thermogravimetric analysis results in Figures S2 and S3 show that 60−90% of constituent compounds in the biocrude oil and HTL-AP samples have a boiling point ≤280 °C, indicating that the implemented GC−MS protocols could detect most constituent compounds in biocrude oil and HTL-AP.

Selected hydro-char samples, which were finely ground and screened to get ultra-fine particle sizes ≤20 μm, were analyzed for the organic- and mineral-phase compositions using quantitative X-ray diffraction (XRD). The XRD analysis was performed at room temperature over 2θ range of 10−80° with a step size of 0.01° using a Bruker D8 Advance ECO diffractometer (1 kW/40 kV/25 mA, Cu Kα radiation at 1.5406 Å). The divergent beam slit, detector slit, position-sensitive detector opening, and discriminator range were set at 0.6 mm, 9 mm, 2.747, and 0.110−0.250 V, respectively. The acquired XRD pattern was processed on MDI Jade 7.8.2 following the whole pattern fitting (WPF) and Rietveld refinement technique[44] based on the PDF-4/organic and PDF-4/mineral database.[45]

2.3. Experimental Design and Data Analysis. *2.3.1. Central Composite Design.* The HTL experimental programs in this study were divided into three parts: central composite design (CCD), validation, and evaluation experiments. The triplicated CCD experiments consisted of 8 factorial points, 6 axial points, and 1 six-folded center point. The presence of axial and center points allows the curvature (quadratic effects) in the responses to be modeled accurately using a full quadratic regression. The characteristic orthogonal block and rotatability of CCD allow the model terms and block effects to be predicted independently, the variation in the regression coefficients to be minimized, and the prediction variance at all points to be constant. The significances of the established quadratic model are the ability to map a region of a response surface and understand how particular changes in independent variables affect the responses of interest. Moreover, the levels of independent variables that optimize multiple responses and ultimately meet the research objectives can be specified.

A complete CCD matrix is given in Table S4 in the Supporting Information. A set of natural values for each independent variable according to the factor level scale (coded units) are given in Table 2.

Table 2. Factor Levels for CCD Experiments (AW: Acid Whey and MD: Manure Digestate)

independent variables		factor levels				
		−2	−1	0	1	2
X_1:	temperature (°C)	280	300	320	340	360
X_2:	time (min)	10	20	30	40	50
X_3:	AW/MD	0	0.5	1	1.5	2

Reaction temperature and reaction time between 280 and 360 °C and 10 and 50 min, respectively, were selected because they allowed a complete conversion of polysaccharides and lignin and gave a maximum yield of biocrude with a low heteroatom content. A mixing ratio of acid whey to manure digestate (here in referred to as "AW/MD") between 0 and 2 was selected because (1) the lowest ratio serves as a base case scenario and (2) the highest ratio provides an optimal balance between the amount of acid whey added and the lowest achievable pH around 5.3.

2.3.2. Regression Analysis and Data Visualization. Regression analysis was performed by fitting a quadratic regression model in a coded unit (see eq 12) with data on measured responses from the CCD experiments (see Tables S5−S7 in the Supporting Information). The coded unit denotes that the value of independent variables was standardized on the factor level scale, that is, from −2 to 2. The fitting process utilized Minitab 21.1.0 to determine the coded value of regression coefficients of only statistically significant terms ($p < 0.05$) while maintaining the hierarchical form. The hierarchical form means that lower-order terms constructing the statistically significant higher-order terms are kept in the equation regardless of their significance.

$$Y = \beta_0 + \sum_{j=1}^{n} \beta_j X_j + \sum_{j=1}^{n} \beta_{jj} X_j^2 + \sum_{j=1}^{n-1} \sum_{k=j+1}^{n} \beta_{jk} X_j X_k \quad (12)$$

where Y is the response variable, β_0 is the intercept, X is a set of three ($n = 3$) independent variables defined in Table 2, and β_j, β_{jj}, and β_{jk} are fitted coefficients of linear, quadratic, and interaction terms, respectively.

Subsequently, the performances of the generated regression equation were assessed based on R^2, R^2(pred.), and lack-of-fit p-value. Satisfactory statistical performances are defined as R^2 close to 1, R^2(pred.) that is not too far below R^2, and the lack-of-fit $p > 0.05$. These criteria demonstrate that the model shows a good fit with experimental data without overfitting the random noise. In addition, they allow us to compare the value of coded coefficients of statistically significant terms in the equation ($p < 0.05$; see the p-values of significant terms in Tables S11−S18) in order to describe the relative effects of the independent variables on measured response variables.

The profile of each response variable (e.g., linear, pure quadratic, and positive/negative two-factor interactions) with its local or global critical points (e.g., maxima, minima, or saddle points) was visualized using contour plots. The contour plots were created using the developed regression equations by varying a pair of statistically significant independent variables while keeping the other independent variable steady at the center-point value. The center-point value can be found in Table 2 under factor level zero.

2.3.3. Multi-Response Optimization. Response surface optimization based on the developed regression models was performed in Minitab 21.1.0 by employing the desirability function approach to achieve the targeted outcomes, that is, maximum carbon/energy recovery in biocrude oil, low biocrude heteroatom content; minimal hydro-char yield; maximal Mg, NH_3-N, and P yields; and minimal Ca yield in HTL-AP. The exponential desirability function determined the optimal reaction temperature and time for various mixing ratios of acid whey and manure digestate by first translating the value of each optimized response, which were obtained from the corresponding regression models, into a value between 0 (undesirable) and 1 (desirable).[46] These individual desirability values were geometrically averaged with an equal weighting factor to obtain the composite desirability value. The desirability function maximized the composite desirability as close as possible to 1 (i.e., to achieve the desired overall metric) by iteratively changing the value of temperature and time within the investigated ranges.

2.3.4. Validation and Evaluation Experiments. To validate the optimization results, co-liquefaction feedstocks with different AW/MD mixing ratios were processed using the optimized reaction temperature and time in triplicated HTL experiments. Subsequently, a set of optimized process conditions with the highest composite desirability value (i.e., the highest biocrude energy recovery and nutrient yield in HTL-AP) was employed in triplicated HTL evaluation experiments. The evaluation experiments employed a feedstock mixture that was acidified with acetic acid to pH 3.5, 4, 4.5, and 5. The goal of these experiments was to evaluate how many, if needed, acetic acid should be added into the co-liquefaction feedstock.

3. RESULTS AND DISCUSSION

Our structure is intended to first describe the interpretation results of regression analysis of experimental data from the CCD experiment. This includes the description of the effects of process variables on the formation of products, biocrude energy recovery, and elemental distributions between the product phases, accompanied by mechanistic explanations in

https://doi.org/10.1021/acs.energyfuels.2c03860
Energy Fuels XXXX, XXX, XXX−XXX

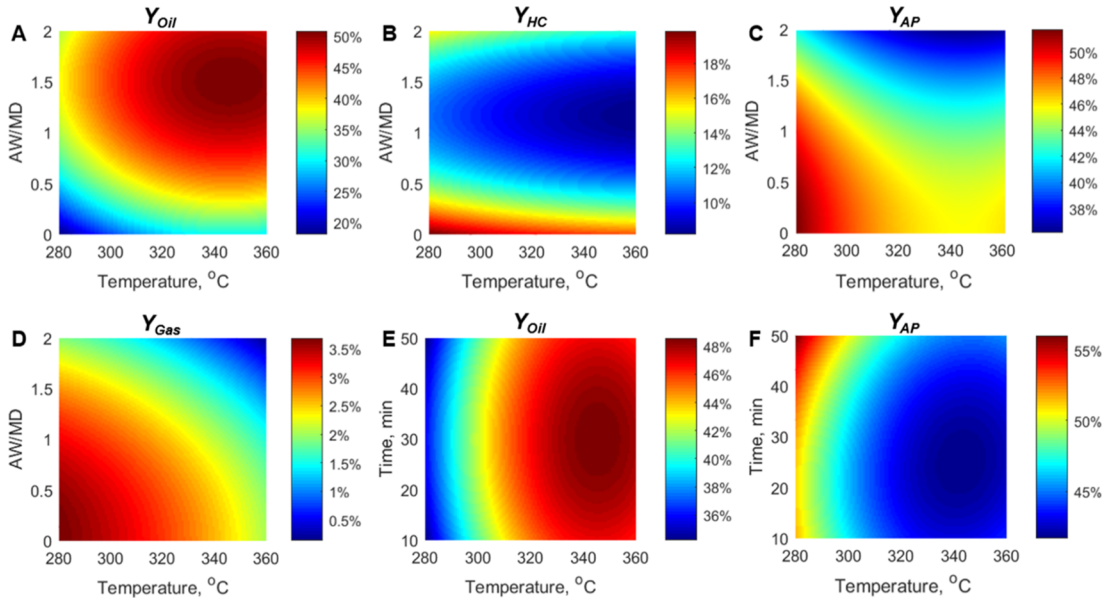

Figure 1. Representative contour plots for product yield: (A) Y_{Oil}, (B), Y_{HC}, (C) Y_{AP}, (D) Y_{Gas}, (E) Y_{Oil}, and (F) Y_{AP}. The colormap shows the value of the corresponding response variable. The *X*-axis and *Y*-axis show the investigated range of value of two statistically significant independent variables. A complete sets of contour plots for product yield can be found in Figures S5−S8 (Supporting Information).

Section 3.1. The mechanistic explanations are provided by combining comparative literature study of well-documented reactions with the chemical composition analysis using GC−MS for biocrude oil and aqueous-phase coproduct and XRD for hydro-char. Subsequently, Section 3.2 presents a range of optimal process conditions for the co-liquefaction that maximize the biocrude energy recovery and nutrient yield in the aqueous phase from feedstock mixtures with different compositions. Validation of the multi-response optimization results and the prominent reaction mechanisms from the corresponding optimum process conditions are also discussed. Ultimately, Section 3.3 discusses the evaluation results of the necessity of adding acetic acid into co-liquefaction feedstock after applying optimal process conditions determined in Section 3.2.

3.1. Effects of Process Conditions on HTL Product Characteristics. In general, the statistical performances of the developed regression models were satisfactory according to R^2 values from 86.51 to 99.88%, R^2(pred.) values from 76.37 to 99.78%, and lack-of-fit *p*-values from 0.138 to 0.424 (see Tables 3−5). Specifically, these values indicated that the model did not overfit the experimental data noise and can predict accurately using a new observation.

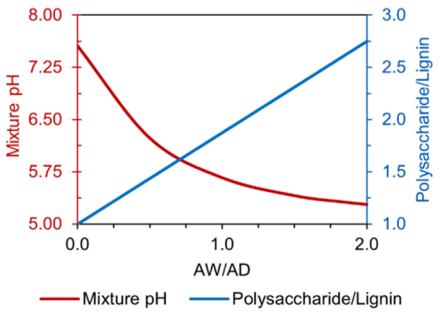

Figure 2. Profile of feedstock pH and polysaccharide-to-lignin ratio for acid whey and manure digestate mixtures.

3.1.1. Product and Carbon Yield. Biocrude oil was the product phase with the highest mass yield (24.01−46.47%), followed by aqueous-phase coproduct (42.3−54.14%), hydro-char (7.11−26.46%), and gas (1.5−4.38%). Similarly, the highest carbon yield was observed in biocrude oil (41.81−77.63%), followed by hydro-char (7.13−43.34%), aqueous-phase coproduct (9.08−21.88%), and gas (1.09−3.44%). The mass yield and carbon yield of each product phase had the same trend with the increasing reaction temperature, reaction time, and mixing ratio of acid whey to manure digestate (AW/MD) according to the profile of coded coefficient values in Table 3. This result was expected because carbon is the backbone of constituent compounds of the HTL products.[47] Therefore, the following discussion on the product yield distribution is also applicable for carbon yield distribution.

The AW/MD was the most significant factor, as evidenced by the highest value for the linear and quadratic term coefficients. A quadratic effect of AW/MD was identified for Y_{Oil}, yielding a maxima at AW/MD of 1.5 (see Figure 1A). Increasing the AW/MD from 0 to 1.5 raised polysaccharide content of feedstock mixture linearly and decreased the pH of feedstock mixture exponentially, that is, from pH 7.1 to 5.5 (see Figure 2). The decreasing feedstock pH to 5.5 enhanced the conversion of polysaccharides into biocrude oil due to higher selectivity for the formation of pyrones, cyclic C_5-ketones, and furandiones (see Table S19) via dehydration of polysaccharides' monomers into 5-HMF and furfural[48] followed by isomerization,[49,50] Piancatelli rearrangement,[49] and cyclization,[51] respectively. In addition, a feedstock pH of around 5.5 has been reported to induce 5-HMF rehydration[52] and lignin acidolysis[53] with formic acid and formaldehyde as the side products, respectively. These two compounds may facilitate reductive depolymerization of lignin and deactivation of reactive sites of the aromatic rings,[28,54] which resulted in the formation of oily monomers with the cyclic C_6-ketone, dioxane, dioxolane, and pyran structures (see Table S19).

At AW/MD > 1.5, feedstock pH was lower than 5.5, enhancing repolymerization of biocrude components into

https://doi.org/10.1021/acs.energyfuels.2c03860
Energy Fuels XXXX, XXX, XXX−XXX

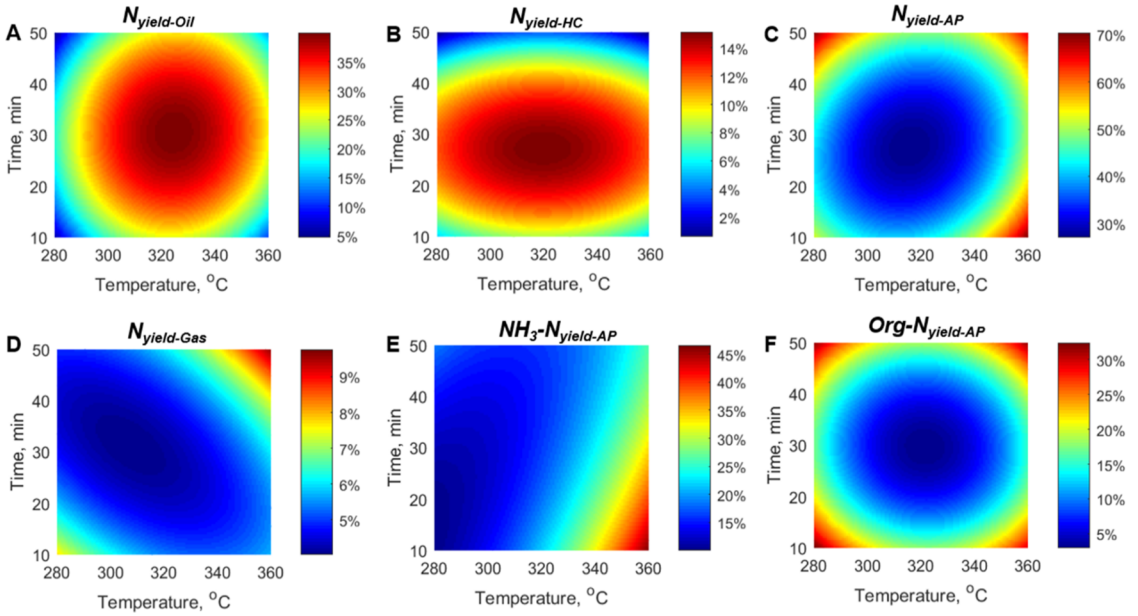

Figure 3. Representative contour plots for nitrogen yield: (A) $N_{yield\text{-}oil}$, (B), $N_{yield\text{-}HC}$, (C) $N_{yield\text{-}oil}$, (D) $NH_3\text{-}N_{yield\text{-}AP}$, (E) $Org\text{-}N_{yield\text{-}AP}$, and (F) $N_{yield\text{-}gas}$. The colormap shows the value of the corresponding response variable. The *X*-axis and *Y*-axis show the investigated range of the values of two statistically significant independent variables. Complete sets of contour plots for nitrogen yield can be found in Figures S13−S18 (Supporting Information).

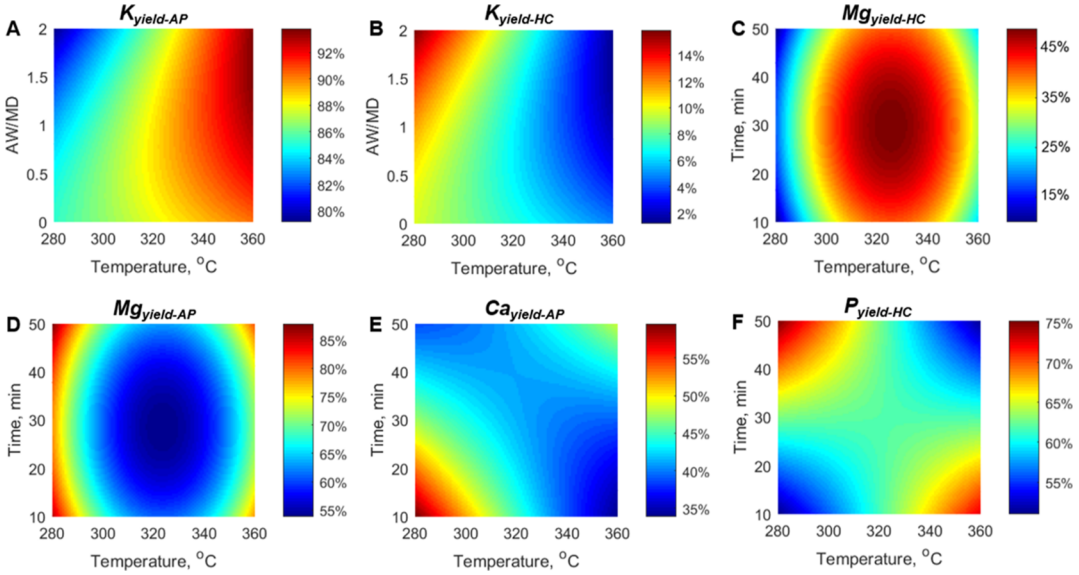

Figure 4. Representative contour plots for nutrient yield: (A) $K_{yield\text{-}AP}$, (B) $K_{yield\text{-}AP}$, (C) $Mg_{yield\text{-}HC}$, (D) $Mg_{yield\text{-}AP}$, (E) $Ca_{yield\text{-}AP}$, and (F) $P_{yield\text{-}HC}$. The colormap shows the value of the corresponding response variable. The *X*-axis and *Y*-axis show the investigated range of values of two statistically significant independent variables. Complete sets of contour plots for nutrient yield can be found in Figures S19−S26 (Supporting Information).

hydro-char and therefore reducing Y_{oil}. This result was confirmed by an increase in Y_{HC} at AW/MD > 1.5 (see Figure 1B). The detected organic phases in the hydro-chars by XRD included 2-amino-4-(2-methoxyphenyl)-7,7-dimethyl-3-nitro-4,6,7,8-tetrahydro-5*H*-chromen-5-one, 1,2-bis(2,6-dichlorobenzylidene)hydrazine, *N*,*N*-dimethyl-4-nitroaniline, 2-(4-hydroxyphenyl)acetonitrile, polyaniline, and 1*H*-1,2,4-triazole-3,5-diamine. This organic-phase composition of hydro-char showed that phenols, hydroxymethyl phenols, methoxyphenols, and hydrazines contained in the biocrude oil (see Table S19) were responsible for the increase in Y_{HC} at AW/MD > 1.5 via 1,3-dipolar cycloaddition,[55] Michael addition,[56] amination,[57] and oxidative polymerization.[58]

Meanwhile, the Y_{AP} and Y_{gas} stabilized around 50% and 4% at an AW/MD of 0−0.6, respectively, after which both Y_{AP} and Y_{gas} continuously decreased at AW/MD > 0.6 (see Figure 1C,D). A significantly higher acidity provided by AW/MD > 0.6 blocked the alkaline degradation pathway of cellulose and lignin (e.g., via retro-aldol condensation)[48] into aqueous aliphatics (see Table S20), which decreased the Y_{AP}. With less availability of short-chain aliphatics in the HTL-AP, the gas formation (Y_{gas}) was consequently lower.

https://doi.org/10.1021/acs.energyfuels.2c03860
Energy Fuels XXXX, XXX, XXX−XXX

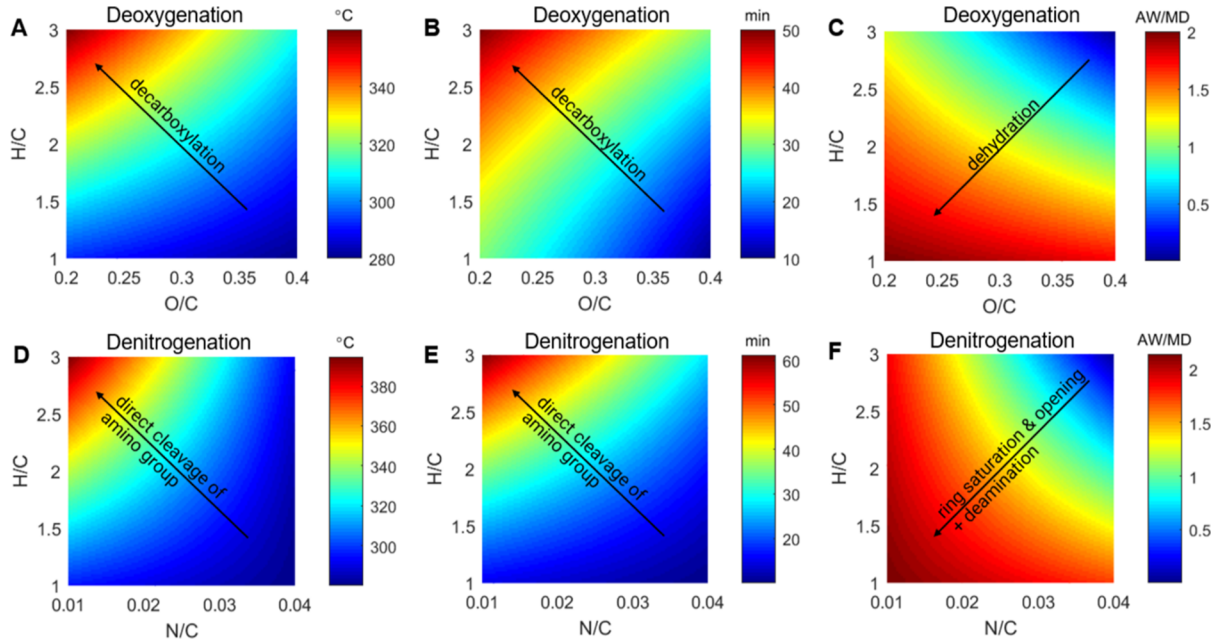

Figure 5. Van Krevelen diagram illustrated as contour plots for showing deoxygenation and denitrogenation mechanisms of biocrude oil at different reaction temperatures (A,D), reaction times (B,E), and AW/MD mixing ratios (C,F). The colormap indicates the value of reaction temperature, reaction time, or AW/MD mixing ratio. The *X*-axis and *Y*-axis represent the O/C or N/C and H/C atomic ratios, respectively.

Table 3. Regression Models for Product Yield, Carbon Yield, ER_{oil}, and HHV_{oil} with Coded Coefficients Truncated to Three Decimal Places (See Tables S5, S8, S9, and S12 in the Supporting Information for Untruncated Coded and Uncoded Coefficient Values)

	measured responses									
terms	Y_{oil}	Y_{HC}	Y_{AP}	Y_{Gas}	$C_{yield\text{-}oil}$	$C_{yield\text{-}HC}$	$C_{yield\text{-}AP}$	$C_{yield\text{-}gas}$	ER_{oil}	HHV_{oil}
constant	46.710	9.163	46.610	1.277	70.850	12.370	18.310	1.897	63.141	31.332
T	3.000	−0.660	−2.268	−0.468	4.769	−0.848	−1.134	−0.390	4.598	2.117
T	−0.020	−1.758	0.763	−0.407	0.069	−3.533	0.381	−0.339	1.210	1.213
AW/MD	4.440	−1.070	−4.031	−0.504	3.327	−1.886	−2.016	−0.420	7.689	0.994
T^2	−1.200	0.120	0.980	−0.048	−2.000	0.952	0.490	−0.040	−0.158	0.556
t^2	−0.420	−0.290	0.550	0.033	−0.608	−0.295	0.275	0.028	0.767	0.469
$(AW/MD)^2$	−2.228	1.689	−1.025	−0.124	−4.102	2.646	−0.513	−0.103	−0.999	0.666
$T \times t$			−0.180	0.180	−0.092		−0.090	0.150	−0.071	−0.193
$T \times (AW/MD)$			0.006	−0.006	−0.323	0.100	0.003	−0.005	0.977	0.217
$t \times (AW/MD)$			0.158	0.158	−0.096		0.079	0.131	0.557	0.344
R^2 (%)	99.75	93.50	92.07	86.51	95.55	92.06	91.65	89.73	96.10	93.28
R^2(pred.) (%)	90.53	89.66	84.93	76.37	83.54	87.92	84.14	82.50	86.59	89.23
lack-of-fit's p	0.278	0.283	0.252	0.214	0.189	0.180	0.193	0.194	0.198	0.209

The reaction temperature showed a negative and positive quadratic effect on Y_{Oil} and Y_{AP}, respectively, and a negative linear effect on Y_{HC} and Y_{gas}. Figure 1 shows that increasing the temperature from 280 to 345 °C increased the Y_{oil} and decreased the Y_{HC}, Y_{AP}, and Y_{gas}. This result indicated that the selectivity of biocrude formation was improved at higher temperatures due to more activated endothermic biocrude oil-forming reactions.[59] According to the detected compounds in biocrude oil (see Table S19), the endothermic reactions included (1) oxidative degradation of lignins into biphenyls[60] (i.e., precursors for polyaromatic hydrocarbons via cyclization and dehydration), (2) oxidation-benzoylation of benzoic acids into benzophenone and anthracenes,[61] (3) condensation-dehydration of erythrose with pyruvic acid into quinic acid,[62] and (4) Fischer indolization involving phenylhydrazines and carbonyl compounds derived from polysaccharides.[63]

From 345 to 360 °C, Y_{oil} and Y_{AP} stabilized around 48 and 40% (see Figure 1E,F), respectively, and Y_{HC} and Y_{gas} continuously decreased (see Figure 1B,D). The relatively constant Y_{oil} and Y_{AP} indicated that the enhanced formation of biocrude oil was balanced by its partial decomposition into aqueous organics, for example, via aromatic or aliphatic cleavage, decarboxylation, and deamination. The decreasing Y_{gas} implied that the formed aqueous organics were chemically more stable and more resistant to decomposition into gas products, for example, acetic acid, cinnamic acid, phenylacetaldehyde, *p*-cresol, and benzidine (see Table S20). The decrease in Y_{HC} showed that hydro-char formation was increasingly inhibited because repolymerization of lignin monomers was blocked by cyclic acetalization and hydroxymethylation of the aromatic ring.[28] This interpretation was confirmed by the presence of 4-(hydroxymethyl)phenol, 1,3-benzodioxane-5-ol, and 5-(1-propenyl)-1,3-benzodioxole in

https://doi.org/10.1021/acs.energyfuels.2c03860
Energy Fuels XXXX, XXX, XXX−XXX

Table 4. Regression Models for Nitrogen Yield with Coded Coefficients Truncated to Three Decimal Places (See Tables S6 and S10 in the Supporting Information for Untruncated Coded and Uncoded Coefficient Values)

	measured responses					
terms	$N_{yield\text{-}oil}$	$N_{yield\text{-}HC}$	$N_{yield\text{-}AP}$	$NH_3\text{-}N_{yield\text{-}AP}$	org-$N_{yield\text{-}AP}$	$N_{yield\text{-}gas}$
constant	39.820	15.610	40.180	27.640	12.950	4.131
T	1.740	−1.020	−1.060	−0.720	−0.320	0.360
T	0.150	0.170	−0.450	−0.690	0.300	0.173
AW/MD	6.625	4.615	−12.210	−11.110	−0.940	0.867
T^2	−4.280	−0.760	4.720	1.400	3.320	0.320
t^2	−3.410	−1.480	4.490	0.660	3.840	0.400
$(AW/MD)^2$	−1.935	1.550	0.425	−3.062	3.488	−0.040
$T \times t$	0.300	0.820	−1.540	−1.740	0.200	0.420
$T \times (AW/MD)$	0.300	−0.180	−0.040	−0.450	0.420	−0.090
$t \times (AW/MD)$	0.305	−0.185	−0.025	−0.105	0.080	−0.094
R^2 (%)	94.38	95.99	98.44	90.19	96.44	88.03
R^2(pred.) (%)	90.32	86.39	88.04	81.36	88.76	77.27
lack-of-fit's p	0.424	0.415	0.413	0.377	0.203	0.338

biocrude oil (see Table S19) and 3,5-dihydroxycinnamic acid, 3,5-dihydroxybenzoic acid, and 5-*tert*-butylpyrogallol in HTL-AP (see Table S20).

Y_{oil} and Y_{AP} showed a negative and positive quadratic dependence on the reaction time, respectively. Y_{oil} was strongly correlated with Y_{AP} because an increase in Y_{oil} was followed by a decrease in Y_{AP}, and vice versa. Moreover, the same reaction time was observed for maxima of Y_{oil} and minima of Y_{AP}, that is, at 30 min. Meanwhile, Y_{HC} and Y_{gas} continuously decreased at prolonged reaction times. These results suggested that 345 °C, 30 min, and an AW/MD of 1.5 were ideal for the highest Y_{oil} while keeping the Y_{AP}, Y_{HC}, and Y_{gas} as low as possible.

3.1.2. Nitrogen Yield. Nitrogen was mostly recovered as NH_3-N and Org-N in HTL-AP with the yield ranging from 7.03 to 41.31% and from 9.85 to 27.39%, respectively. Moreover, $N_{yield\text{-}oil}$, $N_{yield\text{-}HC}$, and $N_{yield\text{-}gas}$ were in the range of 14.7−46.5, 11.00−30.39, and 1.43−4.98%, respectively.

Table 4 shows that the AW/MD was the most important factor with a strongly positive linear correlation with $N_{yield\text{-}oil}$ and $N_{yield\text{-}HC}$ and a highly negative linear correlation with $N_{yield\text{-}AP}$ and $N_{yield\text{-}gas}$. The increasing trend of $N_{yield\text{-}oil}$ with AW/MD (see Figure S13) was attributed to the formation of N-heterocyclics, as shown by the biocrude chemical composition in Table S19. Higher AW/MD increased the acidity and total polysaccharide content of the feedstock, catalyzing the conversion of reducing sugars into α-dicarbonyls, α-hydroxycarbonyls, and benzoic acids during HTL. Through the acid-catalyzed reactions including the Paal−Knorr,[64] Hantzsch,[65] Fischer,[66] and Letts[67] reactions, these compounds may react with primary amine/NH_3 forming pyrroles, pyridines, indoles, and cyanohydrins, respectively. The Paal−Knorr reaction formed pyrroles via the condensation of α-dicarbonyls with NH_3, while the Hantzsch reaction produced pyridines via the condensation of α-hydroxycarbonyls with primary amines. Similarly, indole formation via Fischer mechanism was a condensation reaction, which involved phenylhydrazines and α-dicarbonyls/α-hydroxycarbonyls. The phenylhydrazine may originate from the condensation of lignin-derived phenols with hydrazine. The hydrazine may be obtained from the hydrolysis of 1,2-bis(diphenyl-methylene)-hydrazine, a product of NH_3 condensation with benzoic acid-derived benzophenone. Meanwhile, the Letts reaction involves a mechanism of cyanide addition to an α-dicarbonyl/α-hydroxycarbonyl, forming cyanohydrin derivatives of benzaldehyde, for example, mandelonitrile. These mechanisms for N-fixation were confirmed by the presence of corresponding reaction products in biocrude oil (see Table S19) and by the negative linear correlation of $NH_3\text{-}N_{yield\text{-}AP}$ and Org-$N_{yield\text{-}AP}$ with AW/MD (see Table 4).

The increasing trend of $N_{yield\text{-}HC}$ with AW/MD (see Figure S14) was associated with the precipitation of N-heterocyclics, which were initially produced in the biocrude oil. The precipitation may occur through the coupling reaction, oxidation, cycloaddition, oxazolation, and regioselective ethoxycarbonylation with ring closure. These proposed reaction mechanisms were supported by the XRD detection of the organic phase in the hydro-char that included 2-(5-phenyl-1,3,4-oxadiazol-2-yl)benzoic acid, ethyl-1′,3′,3′-trimethyl-8-nitrospiro[chromene-2,2′-indoline]-5′-carboxylate, 5-formyl-1*H*-pyrrole-2-carboxylic acid, 3,3-diethyl-5-methylpiperidine-2,4-dione, and indole-2-carboxylic acid·3,5-dinitrobenzoic acid (see Table S21). Detailed mechanisms of the formation of these products have been explained in the literature.[68]

The reaction temperature and time provided quadratic effects on the nitrogen yield in all the product phases. The global maxima of $N_{yield\text{-}oil}$ and $N_{yield\text{-}HC}$ and the global minima of $N_{yield\text{-}AP}$ and $N_{yield\text{-}gas}$ were located at the same location, that is, 320 °C and 30 min (see Figure 3A−D). Increasing the reaction temperature from 280 to 320 °C and extending the reaction time from 10 to 30 min favored the endothermic Paal−Knorr, Hantzsch, and Fischer reactions, which enhanced the formation of pyrroles, pyridines, and indoles in the biocrude oil and therefore higher $N_{yield\text{-}oil}$. Moreover, the increased formation of these compounds in biocrude oil may lead to higher $N_{yield\text{-}HC}$ because they may repolymerize and precipitate as complex N-heterocyclics in the hydro-char.[69] The detected N-heterocyclics in the hydro-char by XRD included *N*-methyl-2-(naphtho[2,3-*d*][1,3]dioxol-6-yl)-benzamide, 2,5-di(pyridin-2-yl)pyrazine-1-oxide, 6,8-dimethyl-4-nitro-7,8-dihydro-4*H*-8λ4-pyrazolo[1,5-*a*]pyrimidin-3-amine, and 3-(*tert*-butyl)imidazolidine-2,4-dione (see XRD results in Table S21). The existence of hydantoin, benzamide, and azaarene functional groups in the chemical structure of these organic compounds suggested that N-fixation in hydro-char was controlled by Friedel−Crafts carboxamidation of arenes,[70] Bucherer−Bergs reaction,[71] and Dieckmann cyclization,[72] respectively, at higher temperatures and longer reaction

https://doi.org/10.1021/acs.energyfuels.2c03860
Energy Fuels XXXX, XXX, XXX−XXX

Table 5. Regression Models for Nutrient Yield with Coded Coefficients Truncated to Three Decimal Places (See Tables S7 and S11 in the Supporting Information for Untruncated Coded and Uncoded Coefficient Values)

	measured responses								
terms	$P_{yield\text{-}AP}$	$P_{yield\text{-}HC}$	$K_{yield\text{-}AP}$	$K_{yield\text{-}HC}$	$Ca_{yield\text{-}AP}$	$Ca_{yield\text{-}HC}$	$Mg_{yield\text{-}AP}$	$Mg_{yield\text{-}HC}$	ΔpH_{liq}
constant	36.670	61.940	93.510	6.495	41.390	51.280	54.020	40.710	−1.057
T	0.420	−0.340	2.446	−2.446	−1.980	1.520	−1.640	0.600	−0.168
T	−0.430	0.300	0.070	−0.070	−0.760	0.620	0.660	−0.020	−0.220
AW/MD	17.890	−17.360	−0.338	0.338	9.070	−8.160	−4.240	6.840	−0.117
T^2	−0.080	0.080	−0.040	0.040	0.480	−0.440	5.240	−1.200	0.020
t^2	−0.060	0.060	0.710	−0.710	0.470	−0.430	2.060	−0.420	−0.001
$(AW/MD)^2$	0.912	−0.885	−0.315	0.315	−1.970	1.773	0.815	−1.627	0.019
$T \times t$	2.940	−2.860			2.220	−2.000			−0.004
$T \times (AW/MD)$			0.593	−0.593					−0.004
$t \times (AW/MD)$									−0.006
R^2 (%)	99.88	95.79	97.48	90.46	95.03	96.54	93.01	92.66	91.56
R^2(pred.) (%)	99.78	90.44	95.22	85.35	90.55	90.34	86.72	84.31	83.14
Lack-of-fit's p	0.283	0.248	0.232	0.200	0.178	0.232	0.138	0.203	0.135

times. The increasing $N_{yield\text{-}oil}$ and $N_{yield\text{-}HC}$ resulted in a decreasing trend of $N_{yield\text{-}AP}$. With lower $N_{yield\text{-}AP}$, the potential loss of nitrogen from the aqueous to the gas phase was reduced and therefore $N_{yield\text{-}Gas}$ decreased.

A different phenomenon occurred when the reaction temperature and time increased beyond 320 °C and 30 min. Under these conditions, $N_{yield\text{-}oil}$ and $N_{yield\text{-}HC}$ continuously decreased while $N_{yield\text{-}AP}$ and $N_{yield\text{-}gas}$ continuously increased. The decrease in $N_{yield\text{-}oil}$, which consequently lowered the $N_{yield\text{-}HC}$, was caused by the N removal from biocrude oil. The N-removal process was initiated by the aromatic saturation and ring opening of N-heterocyclics into aliphatic amines. The amine group was readily cleaved to yield aliphatic alkanes in biocrude oil and released N as NH_3 into HTL-AP.[73] This mechanism was confirmed by the detected intermediate and final products in biocrude oil (e.g., 1-ethyl piperazine, 2,6-dimethylpiperidine, 3-methyl indoline, 1-methyl pyrrolidine, pentane, 1-phenyl-1-butene, and 2,4-dimethyl-2,3-pentadiene; see Table S21) and in HTL-AP, for example, 1-butanamine, 1-pentanamine, and benzylamine (see Table S20). The increased production of amines (i.e., the intermediates of denitrogenation of biocrude oil after the ring opening step) and NH_3-N in HTL-AP contributed toward the increasing trend of $N_{yield\text{-}AP}$ at reaction temperatures >320 °C and reaction times >30 min (see Figure 3E,F). In addition, amines and NH_3-N distributed in HTL-AP may be partially decomposed and vaporized into the gas phase under these conditions, increasing the $N_{yield\text{-}gas}$.

3.1.3. Inorganic Yield. Precipitation in the hydro-char and mineral dissociation in the HTL-AP were two primary mechanisms that controlled the partitioning of inorganics during co-liquefaction of acid whey and manure digestate. The total yield of each inorganic element in these two products was close to 100%. The $P_{yield\text{-}AP}$, $Ca_{yield\text{-}AP}$, $Mg_{yield\text{-}AP}$, and $K_{yield\text{-}AP}$ were in the range of 14.41−72.44, 15.17−53.47, 43.39−73.27, and 91.06−98.28%, respectively, whereas the $P_{yield\text{-}HC}$, $Ca_{yield\text{-}HC}$, $Mg_{yield\text{-}HC}$, and $K_{yield\text{-}HC}$ were in the range of 26.73−83.02, 41.88−76.34, 30.79−46.23, and 2.70−9.85%, respectively. The inorganic yield in biocrude oil was insignificant because the measured ash content was very low (0−0.4%; see Table S4), consistent with an earlier study on HTL of acid whey.[32]

Higher AW/MD increased the acidity of the reaction mixture, solubilizing more P, Ca, and Mg minerals in the HTL-AP. This solubilization provided higher $P_{yield\text{-}AP}$, $Ca_{yield\text{-}AP}$, and $Mg_{yield\text{-}AP}$ and therefore lower $P_{yield\text{-}HC}$, $Ca_{yield\text{-}HC}$, and $Mg_{yield\text{-}HC}$ at higher AW/MD. In contrast, higher AW/MD decreased $K_{yield\text{-}AP}$ and increased $K_{yield\text{-}HC}$ (see Figure 4A,B). Since the XRD pattern of the hydro-chars did not show any K minerals, these results implied that higher AW/MD generated hydro-char with a more activated surface. The activated surface enabled the physisorption of K in hydro-char and therefore higher $K_{yield\text{-}HC}$. The physisorption was assumed to be a reversible exothermic process due to the negative linear and negative quadratic correlation of $K_{yield\text{-}HC}$ with reaction temperature and time, respectively (see Table 5).

The reaction temperature and reaction time showed a quadratic effect on $Mg_{yield\text{-}AP}$ and $Mg_{yield\text{-}HC}$. The global maxima for $Mg_{yield\text{-}AP}$ and the global minima for $Mg_{yield\text{-}HC}$ were located at 320 °C and 30 min, as shown by Figure 4C,D. Increasing the reaction severity from 280 °C and 10 min to 320 °C and 30 min solubilized the Mg minerals due to enhanced acid production. The enhanced acid production was confirmed by the negative correlation of ΔpH_{liq} (i.e., pH difference between feedstock mixture and the collected HTL-AP) with the reaction temperature and time (see Figure S33). As the operating conditions increase past 320 °C and 30 min, Mg^{2+} may chelate the CO_2 dissolved in HTL-AP as CO_3^{2-} to reprecipitate as nesquehonite ($MgCO_3{\cdot}3H_2O$) and magnesite ($MgCO_3$) minerals.[74] The formation of these minerals lowered $Mg_{yield\text{-}AP}$ and increased $Mg_{yield\text{-}HC}$.

The reprecipitation phenomenon was also valid to explain the decreasing trend of $Ca_{yield\text{-}AP}$ with the reaction temperature and time, as shown in Figure 4E. Calcite and brushite, the major Ca mineral phases in the co-liquefaction feedstock, were dissociated in the HTL-AP during HTL. Higher reaction severity favored the endothermic reorientation of the dissolved Ca^{2+} into more thermodynamically stable solid Ca minerals in the hydro-chars,[75] for example, troemelite, monetite, β-tricalcium phosphate, and A-type carbonated apatite. This proposed mechanism was confirmed by the XRD patterns in Figure S4.

Figure 4F shows a saddle, where a combination of a lower temperature with a longer reaction time or a higher temperature with a shorter reaction time increased $P_{yield\text{-}HC}$ or in other words reduced $P_{yield\text{-}AP}$. The former condition promoted the precipitation of phosphate as whitlockite ($Ca_9MgHPO_4(PO_4)_6$; see the XRD pattern in Figure S4D),[76] consistent with the increasing trend of $Ca_{yield\text{-}HC}$ and

https://doi.org/10.1021/acs.energyfuels.2c03860
Energy Fuels XXXX, XXX, XXX−XXX

$Mg_{yield\text{-}HC}$ with the reaction temperature and time. The latter condition facilitated the crystallization of phosphate into urea hydrogen phosphate in the hydro-char,[77] as shown by the XRD pattern in Figure S4F.

3.1.4. Biocrude Energy Recovery and Heteroatoms Content. With the $HHV_{feedstock}$, HHV_{oil}, and Y_{oil} in the range of 9.95−15.02, 16.44−26.70, and 24.01−46.47%, respectively, the energy recovered in biocrude oil (ER_{oil}) was 41.81−77.63%. The main effects plots in Figure S36 show that the increasing trend of ER_{oil} with temperature, time, and AW/MD was highly associated with a significant improvement of Y_{oil} (see Section 3.1 for detailed discussion) and HHV_{oil}. The improvement of HHV_{oil} was due to the formation of carbon-rich compounds (see Table S19) and the removal of heteroatoms, that is, oxygen and nitrogen.

The van Krevelen diagrams in Figure 5A,B,D,E show that the deoxygenation and denitrogenation of biocrude oil were controlled by decarboxylation and direct cleavage of the amino/amine group, respectively, at higher temperatures and longer reaction times. The higher reaction severity enhanced the thermal-oxidative scission of carbon−carbon and carbon−nitrogen bonds attached to the −COOH and $-NH_2$ groups, respectively, removing oxygen as CO_2 into the gas phase and nitrogen as NH_3 into the HTL-AP.[78] The resulting products of decarboxylation include aliphatic hydrocarbons with the H/C atomic ratio ranged between 2 and 3 (e.g., *n*-decane, *n*-dodecane, *n*-hexadecane, and *n*-octadecane; see Table S19), as illustrated by Figure 5A,B. Likewise, the direct cleavage of N-heterocyclics with two nitrogen atoms (e.g., pyrazole and pyrazine) resulted in the formation of aliphatic amines with the H/C atomic ratio between 2 and 3 (see Figure 5D,E),[79] for example, propylamine and butylamine (see Table S19).

Meanwhile, at higher AW/MD, deoxygenation and denitrogenation of biocrude oil were controlled by dehydration and deamination pathways (see Figure 5C,D). Higher AW/MD provided significant hydrogen donors through the presence of acids contained in acid whey (e.g., lactic acid) and those derived from polysaccharide decomposition, for example, formic acid and glycolic acid (see Table S20). They may reduce the C═O bond of ketones and aldehydes into C−OH, which was readily dehydrated into aliphatic alkanes (see Figure 5C).[80] In addition, the hydrogen donors may also saturate the N-heterocyclic ring to facilitate ring opening and then deamination, expelling N as NH_3 in HTL-AP (see Section 3.2 for the deamination pathway explanation).[73,79]

3.2. Optimization and Validation of HTL Process Conditions. In general, the optimal reaction temperature and time for co-liquefaction of acid whey and manure digestate were divided into three regions of the AW/MD mixing ratio (see Figure 6). The first region showed that an increase in AW/MD from 0 to 1 required a higher temperature from 338 to 341 °C and a longer reaction time from 41 to 47 min. Higher AW/MD raised the polysaccharide content and lowered the pH of feedstock mixture. These conditions enhanced the formation of oxygenates (e.g., ketones, furandiones, and pyrones) in biocrude oil through acid-catalyzed isomerization, Piancatelli rearrangement, and oxidation of polysaccharide-derived furans.[81] Higher AW/MD also led to the production of more α-dicarbonyls/α-hydroxycarbonyls from reducing sugars. The carbonyl compounds were highly reactive with primary amine/NH_3, forming N-heterocyclics in biocrude oil through the Paal−Knorr, Hantzsch, Fischer, and Letts reactions (see Section 3.2 for a

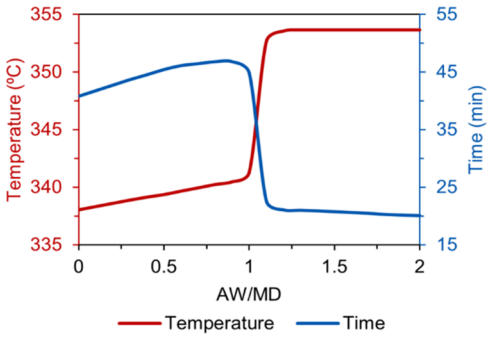

Figure 6. Suggested reaction temperatures and times for AW/MD of 0−2 to achieve the multi-response optimization objectives.

mechanistic explanation). The formation of oxygenates and N-heterocyclics consequently increased the oxygen and nitrogen content of biocrude oil. Therefore, higher reaction temperatures and prolonged reaction times were required to remove oxygen and nitrogen from biocrude oil in order to maximize ER_{oil}. Moreover, higher reaction severity gave a higher nutrient yield in HTL-AP due to enhanced acid production from the decomposition of polysaccharides and lignins (see the profile of ΔpH_{liq} versus temperature and time in Figure S33).

The second region shows that an increase in AW/MD from 1 to 1.1 required a significantly higher temperature from 341 to 354 °C and a much shorter reaction time from 47 to 21 min. Figure 2 illustrates that at AW/MD > 1, the linear increase of the polysaccharide/lignin ratio was not compensated by a commensurate decrease of the pH of the feedstock mixture. This result implied that a larger production of α-dicarbonyls/α-hydroxycarbonyls from polysaccharides, which led to massive N-heterocyclics formation, was not balanced by a comparable increase of H^+ activity required to remove nitrogen via the deamination pathway, that is, aromatic saturation, ring opening, and N-removal as NH_3. Employing much higher temperatures was an alternative solution to remove nitrogen through direct cleavage of the amino/amine group without being preceded by hydrogenation, as illustrated by the van Krevelen diagrams in Figure 5. Moreover, higher temperatures may selectively precipitate Ca in hydro-char (see Table 5 in Section 3.3). Employing a much shorter reaction time minimized NH_3-N fixation in the biocrude oil and blocked the reprecipitation of dissolved Mg and P in the hydro-char as magnesite, urea hydrogen phosphate, and β-tricalcium phosphate minerals (see Subsection 3.3). Therefore, higher NH_3-$N_{yield\text{-}AP}$, lower $Ca_{yield\text{-}AP}$, and higher $P_{yield\text{-}AP}$ and $Mg_{yield\text{-}AP}$ were obtained.

In the third region, AW/MD increased from 1.1 to 2 and the optimum reaction temperature and time stabilized at 354 °C and ∼21 min. Although a higher temperature was favored for heteroatom removal, a reaction temperature of >354 °C initiated partial decomposition of biocrude oil into aqueous-phase organics, as discussed in Section 3.1. Meanwhile, a reaction time of <21 min could not provide an acidity level required for solubilizing minerals in HTL-AP (see the profile of ΔpH_{liq} vs time in Figure S33). Therefore, a reaction temperature and time at 354 °C and ∼21 min were optimal for maximal Y_{oil}, $P_{yield\text{-}AP}$, and $Mg_{yield\text{-}AP}$.

According to the composite desirability results covering the three optimal regions (see Figure S35), the highest biocrude energy recovery and the highest nutrient yield in HTL-AP were given by a reaction temperature of 354 °C, reaction time

https://doi.org/10.1021/acs.energyfuels.2c03860
Energy Fuels XXXX, XXX, XXX−XXX

Table 6. Validation Results for Multi-Response Optimization. (Exp. = Experimental Value and |Diff.| = Absolute Difference between the Predicted and Average Value of Exp.)

	AW/MD 0.3339 °C44 min		AW/MD 1.05347 °C34 min		AW/MD 1.21354 °C21 min		AW/MD 1.6354 °C21 min	
optimized responses	Exp.	|Diff.|	Exp.	|Diff.|	Exp.	|Diff.|	Exp.	|Diff.|
Y_{oil} (%)	37.2 ± 0.2	0.2	49.2 ± 0.3	0.3	49.7 ± 0.2	0.2	50.6 ± 0.7	0.5
ER_{oil} (%)	56.0 ± 0.5	0.6	70.9 ± 0.4	0.4	74.6 ± 0.9	0.9	79.9 ± 0.3	0.6
HHV_{oil}(MJ/kg)	35.3 ± 0.2	0.1	36.1 ± 0.6	0.3	36.8 ± 0.3	0.1	39.1 ± 0.8	0.8
% C_{oil}	54.1 ± 0.6	0.4	56.1 ± 0.2	0.1	57.6 ± 0.5	0.3	58.2 ± 0.7	0.1
% N_oil	0.8 ± 0.1	0.0	0.6 ± 0.2	0.1	1.2 ± 0.2	0.0	1.0 ± 0.1	0.0
% O_oil	29.1 ± 0.4	0.1	29.0 ± 0.6	0.1	28.9 ± 0.3	0.1	29.0 ± 1.0	0.4
Y_{HC} (%)	11.2 ± 0.7	0.8	7.8 ± 0.1	0.1	10.1 ± 0.5	0.5	11.8 ± 0.6	0.9
$P_{yield\text{-}AP}$ (%)	16.6 ± 0.6	0.3	40.6 ± 0.2	0.3	44.9 ± 0.6	3.8	54.9 ± 0.6	0.9
$NH_3\text{-}N_{yield\text{-}AP}$ (%)	36.8 ± 0.2	0.2	27.1 ± 0.4	0.2	29.1 ± 0.4	0.3	15.7 ± 0.1	0.0
$Mg_{yield\text{-}AP}$ (%)	70.1 ± 1.0	0.4	62.0 ± 0.2	0.5	66.0 ± 0.2	0.2	63.7 ± 0.5	0.2
$Ca_{yield\text{-}AP}$ (%)	26.4 ± 0.2	0.2	41.8 ± 0.3	0.4	40.4 ± 0.1	0.1	45.5 ± 0.4	0.4

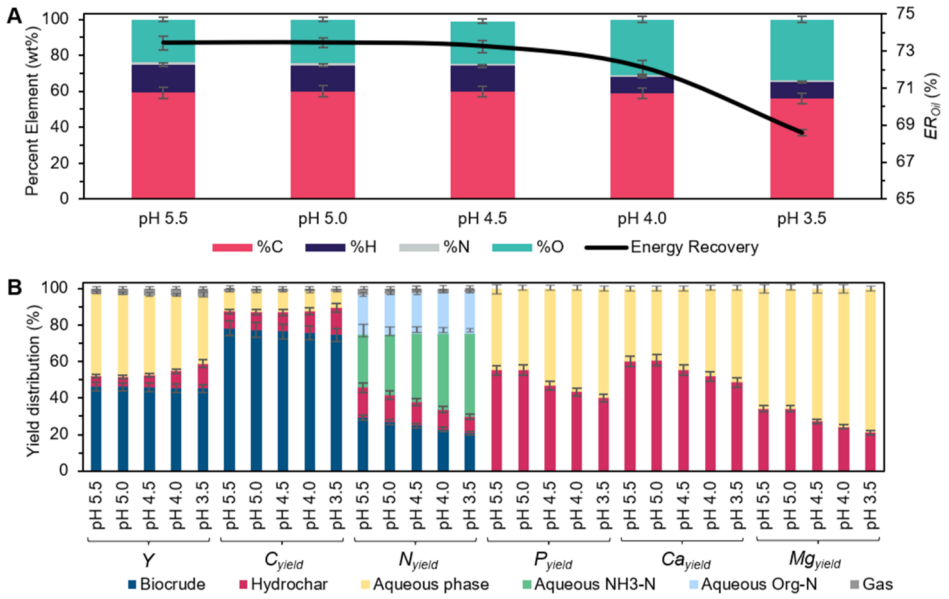

Figure 7. Results from HTL experiments on acid whey and manure digestate mixtures at 354 °C, 21 min, and AW/MD of 1.21 without (pH 5.5) and with (pH 3.5−5) additional pre-acidification using acetic acid: (A) biocrude elemental composition and energy recovery and (B) yield of products and elements.

of 21 min, and AW/MD of 1.21. From the energy recovery aspect, an AW/MD of 1.21 resulted in a feedstock pH of 5.55, allowing the achievement of the highest Y_{oil} (see Section 3.1). Combined with the reaction temperature and time of 354 °C and 21 min, respectively, the maximum biocrude production was accompanied with less NH_3-N fixation and significant heteroatom removal, increasing $NH_3\text{-}N_{yield\text{-}AP}$ and ER_{oil}. From the nutrient yield aspect, an AW/MD of 1.21 provided optimal acidity to dissolve mineral nutrients, yielding maximal $Mg_{yield\text{-}AP}$, $P_{yield\text{-}AP}$, $NH_3\text{-}N_{yield\text{-}AP}$, and $K_{yield\text{-}AP}$. Similarly, a reaction temperature of 354 °C led to the dissolution of more nutrients due to massive acid generation from the hydrothermal decomposition of polysaccharides and lignins. Meanwhile, a reaction time of 21 min retained the dissolved nutrients in the HTL-AP.

These optimization results were verified through triplicated HTL experiments on feedstock mixtures with four different AW/MD mixing ratios (i.e., 0.3, 1.05, 1.21, and 1.6) by employing the suggested reaction temperatures and times. Table 6 shows the negligible differences between the estimated and experimental values of the optimized responses, suggesting high accuracy of the responses' regression models for all sets of combinations of independent variables.

3.3. Comparison with Acetic Acid-Catalyzed HTL. This section evaluates the characteristics of co-liquefaction products without and with the addition of acetic acid into the co-liquefaction feedstock mixture. The applied HTL process conditions were 354 °C, 21 min, and AW/MD of 1.21, that is, equivalent to a feedstock pH of 5.5 without acetic acid addition.

Figure 7 demonstrates that the co-liquefaction feedstock did not require acetic acid addition if the targeted outcome was only recovering carbon/energy in the biocrude. The ER_{Oil} plateaued when feedstock pH dropped from 5.5 to 4.5 with acetic acid addition (see Figure 7A). A significant decrease of ER_{oil} was observed when feedstock pH was <4.5. The ER_{oil} reduction was due to the decrease in % C_{oil} and % H_{oil} and the increase in % O_{oil} (see Figure 7B), leading to lower HHV_{oil}. The change in elemental composition was associated with the enhanced carboxylation of biocrude due to the increasing amount of acetic acid in the feedstock. This was evidenced by (1) the decrease in H/C atomic ratio and the increase in the

https://doi.org/10.1021/acs.energyfuels.2c03860
Energy Fuels XXXX, XXX, XXX−XXX

O/C atomic ratio (see the van Krevelen diagram in Figure S33) and (2) a higher composition of acids and esters in biocrude oil produced from feedstock mixture with a pH of <4.5 (see Table S19). Moreover, more acidic feedstock pH increased Y_{HC}, which is undesirable. Hydro-char may adsorb the biocrude oil during HTL, resulting in the requirement of the post-HTL extraction process and therefore higher operational cost. Hydro-char may also cause partial plugging of the reactor's pressure control valves and piping systems,[82] jeopardizing the HTL process safety.

If the targeted outcomes included high nutrient yield in the HTL-AP, acetic acid would have to be added to the feedstock mixture. Acetic acid was relatively stable until 400 °C. Meanwhile, lactic acid, as the main acid contributor from acid whey, may undergo decarboxylation into acetaldehyde, CO_2, and H_2 at near-supercritical water temperatures.[83] This was confirmed by the absence of lactic acid and the presence of acetaldehyde in the HTL-AP at temperatures ≥320 °C (see Table S20). Adding acetic acid into the feedstock mixture until the feedstock is pH ≤ 4.5 may (1) adequately cover the partial loss of acidity due to the lactic acid decomposition and (2) lead to producing more acids in the reaction medium during HTL through the acidic HTL reaction pathways.[33] As a result, more mineral nutrients were solubilized in the HTL-AP. This was proven by the increasing trend of $P_{yield\text{-}AP}$, $Ca_{yield\text{-}AP}$, and $Mg_{yield\text{-}AP}$ at a feedstock pH of ≤4.5 after being stabilized at a feedstock pH of 5−5.5. In addition, Figure 7B shows that NH_3-$N_{yield\text{-}AP}$ increased at a feedstock pH of ≤4.5, indicating an enhanced deamination of amino acids and nitrogen removal from biocrude oil as NH_3-N in HTL-AP. Considering both energy and nutrient recovery aspects, the most acidic pH after acetic acid addition that could be employed was pH 4.5 to maintain the high biocrude energy recovery while improving the nutrient yield in HTL-AP.

4. CONCLUSIONS

Sustainable resource recovery, particularly carbon and nutrients, from waste byproducts of concentrated animal feeding operations and subsequent milk processing is required to achieve a circular bioeconomy for the dairy industry. This study examined the potential of using hydrothermal co-liquefaction of manure digestate with acid whey to produce energy-rich biocrude oil and a nutrient-rich aqueous-phase coproduct. In the presence of acid whey in the feed mixture, the amount of acetic acid required to catalyze the conversion was lower.

The effects of reaction conditions, including temperature (280−360 °C), reaction time (10−50 min), mixing ratio of acid whey to manure digestate (AW/MD of 0−2), and the amount of acetic acid addition (i.e., measured based on final feedstock pH values ranging from 3.5 to 5.5), were investigated using a comprehensive experimental design to quantify the distribution of products and the fate of elements. Experimental results demonstrated that adding acetic acid to the feedstock mixture with an AW/MD ratio of 1.21 to reach a pH of 4.5 before being processed yielded maximum carbon recovery in biocrude oil (i.e., 75% or equivalent to 73% energy recovery) with less heteroatom content (i.e., 23% O and 1.3% N) and significant nutrient yield in the aqueous-phase coproduct (i.e., 40% NH_3-N, 63% P, 60% Mg, and 45% Ca) when reacted at a temperature of 354 °C for 21 min. An AW/MD of 1.21 raised the content of polysaccharides and hydrogen donors in the feedstock, increasing the biocrude yield through the formation of non-polar species, for example, pyrones, cyclic C_5-ketones, furandiones, cyclic C_6-ketone, dioxanes, dioxolanes, and pyrans. Acetic acid addition to give a feedstock pH of 4.5 adequately compensated for the partial loss of acidity of the reaction medium during HTL due to lactic acid decomposition at near-supercritical water temperatures. This compensation resulted in a higher dissolution of mineral nutrients in the aqueous phase while still maintaining the maximum biocrude energy recovery. A reaction temperature of 354 °C also resulted in a higher heating value of biocrude. Most likely, this was a result of removing heteroatoms via decarboxylation, dehydration, direct cleavage of amino group, and a series of aromatic saturation, ring opening, and deamination utilizing hydrogen donors supplied by acid whey, forming more aliphatic hydrocarbons in biocrude oil. A reaction time of 21 min was sufficient for acid production from the conversion of polysaccharides and lignins during HTL in order to dissolve a significant amount of mineral nutrients in the aqueous phase.

These results suggest that mixing acid whey in the HTL feedstock can not only partially replace acetic acid by contributing acidity to the feedstock mixture but also improve the quantity and quality of biocrude oil through the presence of polysaccharides and hydrogen donors. Moreover, the significant recoverable yield of carbon and nutrient in the biocrude and the aqueous-phase coproduct, respectively, shows the potential of hydrothermal co-liquefaction in mitigating several environmental threats (e.g., global warming, eutrophication of water basin, acidification of ecosystems, and aerosol pollution) caused by uncontrolled emission of carbon and nutrients as a result of the improper management of dairy waste.

Although this study demonstrated that hydrothermal co-liquefaction could be a key process in resource-efficient valorization of biomass for sustainable waste management in the dairy sector, further processing will be required for practical applications. For example, the produced biocrude oil will need to be refined to reach desired "drop-in" fuel quality and the nutrient mixture in the aqueous-phase coproduct will need to be further processed to recover nutrients for reuse.

■ ASSOCIATED CONTENT

Supporting Information

The Supporting Information is available free of charge at https://pubs.acs.org/doi/10.1021/acs.energyfuels.2c03860.

HTL experimental design and protocols; data of measured responses from CCD experiments; feedstock physicochemical characterization procedure; regression models; contour plots of measured responses; GC−MS composition of biocrude oil and aqueous-phase coproduct; quantitative XRD analysis of hydro-char; van Krevelen diagrams of biocrude oil; thermogravimetric analysis results of biocrude oil; and composite desirability profile (PDF)

■ AUTHOR INFORMATION

Corresponding Author

Hanifrahmawan Sudibyo − *School of Chemical and Biomolecular Engineering, Cornell University, Ithaca, New York 14853, United States; Energy Systems Institute, Cornell University, Ithaca, New York 14853, United States; Chemical Engineering Department, Universitas Gadjah Mada, Yogyakarta 55281, Indonesia;* orcid.org/0000-0003-

https://doi.org/10.1021/acs.energyfuels.2c03860
Energy Fuels XXXX, XXX, XXX−XXX

1905-129X; Phone: +62 821-3703-0223; Email: hs987@cornell.edu

Author

Jefferson William Tester − *School of Chemical and Biomolecular Engineering, Cornell University, Ithaca, New York 14853, United States; Energy Systems Institute, Cornell University, Ithaca, New York 14853, United States*

Complete contact information is available at: https://pubs.acs.org/10.1021/acs.energyfuels.2c03860

Author Contributions

H.S.: conceptualization, methodology, formal analysis, investigation, data curation, visualization, and writing—original draft. J.W.T.: conceptualization, writing—review and editing, research supervision, and funding acquisition.

Notes

The authors declare no competing financial interest.

■ ACKNOWLEDGMENTS

This study was supported by the U.S. Department of Energy through their RAPID program with award number DE-EE0007888-9.7, the USDA grant 2019-69012-29905 involving collaborative research between Cornell University and the University of Arkansas, and the Graduate School at Cornell. This study also made use of the Cornell Center for Materials Research (NSF MRSEC DMR-1719875) shared facilities. H.S. also thanks the Fulbright-DIKTI Foundation for their financial support as a doctoral candidate in chemical engineering at Cornell University.

■ REFERENCES

(1) USDA. *Dairy Products June 2020 Highlights*, 2020.
(2) NCBA. Beef Industry Overview. Industry Statistics. https://www.ncba.org/Media/NCBAorg/Docs/industry-statistics_1.pdf (accessed May 17, 2021).
(3) Ipiales, R. P.; de la Rubia, M. A.; Diaz, E.; Mohedano, A. F.; Rodriguez, J. J. Integration of Hydrothermal Carbonization and Anaerobic Digestion for Energy Recovery of Biomass Waste: An Overview. *Energy Fuel.* **2021**, *35*, 17032−17050.
(4) Sudibyo, H.; Shabrina, Z. L.; Wondah, H. R.; Hastuti, R. T.; Purnomo, L.; Budhijanto, C. W.; Budhijanto, W. Anaerobic Digestion of Landfill Leachate with Natural Zeolite and Sugarcane Bagasse Fly Ash as the Microbial Immobilization Media in Packed Bed Reactor. *Acta Polytech.* **2018**, *58*, 57−68.
(5) Halim, L.; Mellyanawaty, M.; Cahyono, R. B.; Sudibyo, H.; Budhijanto, W. Anaerobic Digestion of Palm Oil Mill Effluent with Lampung Natural Zeolite as Microbe Immobilization Medium and Digested Cow Manure as Starter. *AIP Conf. Proc.* **2017**, *1840*, 110003.
(6) Zeshan; Visvanathan, C. Evaluation of Anaerobic Digestate for Greenhouse Gas Emissions at Various Stages of Its Management. *Int. Biodeterior. Biodegrad.* **2014**, *95*, 167−175.
(7) Nishanthi, M.; Vasiljevic, T.; Chandrapala, J. Properties of Whey Proteins Obtained from Different Whey Streams. *Int. Dairy J.* **2017**, *66*, 76−83.
(8) Risberg, K.; Cederlund, H.; Pell, M.; Arthurson, V.; Schnürer, A. Comparative Characterization of Digestate versus Pig Slurry and Cow Manure − Chemical Composition and Effects on Soil Microbial Activity. *Waste Manag.* **2017**, *61*, 529−538.
(9) Carvalho, F.; Prazeres, A. R.; Rivas, J. Cheese Whey Wastewater : Characterization and Treatment. *Sci. Total Environ.* **2013**, *445*−*446*, 385−396.
(10) Nkoa, R. Agricultural Benefits and Environmental Risks of Soil Fertilization with Anaerobic Digestates: A Review. *Agron. Sustain. Dev.* **2014**, *34*, 473−492.
(11) Möller, K.; Müller, T. Effects of Anaerobic Digestion on Digestate Nutrient Availability and Crop Growth: A Review. *Eng. Life Sci.* **2012**, *12*, 242−257.
(12) Le Maréchal, C.; Druilhe, C.; Repérant, E.; Boscher, E.; Rouxel, S.; Le Roux, S.; Poëzévara, T.; Ziebal, C.; Houdayer, C.; Nagard, B.; Barbut, F.; Pourcher, A. M.; Denis, M. Evaluation of the Occurrence of Sporulating and Nonsporulating Pathogenic Bacteria in Manure and in Digestate of Five Agricultural Biogas Plants. *Microbiologyopen* **2019**, *8*, No. e872.
(13) Wang, W.; Lee, D. J. Valorization of Anaerobic Digestion Digestate: A Prospect Review. *Bioresour. Technol.* **2021**, *323*, 124626.
(14) Iocoli, G. A.; Zabaloy, M. C.; Pasdevicelli, G.; Gómez, M. A. Use of Biogas Digestates Obtained by Anaerobic Digestion and Co-Digestion as Fertilizers: Characterization, Soil Biological Activity and Growth Dynamic of Lactuca Sativa L. *Sci. Total Environ.* **2019**, *647*, 11−19.
(15) Dadrasnia, A.; de Bona Muñoz, I.; Yáñez, E. H.; Lamkaddam, I. U.; Mora, M.; Ponsá, S.; Ahmed, M.; Argelaguet, L. L.; Williams, P. M.; Oatley-Radcliffe, D. L. Sustainable Nutrient Recovery from Animal Manure: A Review of Current Best Practice Technology and the Potential for Freeze Concentration. *J. Clean. Prod.* **2021**, *315*, 128106.
(16) Rodionova, M. V.; Bozieva, A. M.; Zharmukhamedov, S. K.; Leong, Y. K.; Chi-Wei Lan, J.; Veziroglu, A.; Veziroglu, T. N.; Tomo, T.; Chang, J. S.; Allakhverdiev, S. I. A Comprehensive Review on Lignocellulosic Biomass Biorefinery for Sustainable Biofuel Production. *Int. J. Hydrogen Energy* **2022**, *47*, 1481−1498.
(17) Stegmann, P.; Londo, M.; Junginger, M. The Circular Bioeconomy: Its Elements and Role in European Bioeconomy Clusters. *Resour., Conserv. Recycl.* **2020**, *6*, 100029.
(18) Prestigiacomo, C.; Scialdone, O.; Galia, A. Hydrothermal Liquefaction of Wet Biomass in Batch Reactors: Critical Assessment of the Role of Operating Parameters as a Function of the Nature of the Feedstock. *J. Supercrit. Fluids* **2022**, *189*, 105689.
(19) Cabrera, D. V.; Labatut, R. A. Outlook and Challenges for Recovering Energy and Water from Complex Organic Waste Using Hydrothermal Liquefaction. *Sustain. Energy Fuels* **2021**, *5*, 2201−2227.
(20) Cabrera, D. V.; Barria, D. A.; Camu, E.; Celis, C.; Tester, J. W.; Labatut, R. A. Enhancing Energy Recovery of Wastewater Treatment Plants through Hydrothermal Liquefaction. *Environ. Sci. Water Res. Technol.* **2023**, DOI: 10.1039/D2EW00752E.
(21) Ghanim, B. M.; Kwapinski, W.; Leahy, J. J. Speciation of Nutrients in Hydrochar Produced from Hydrothermal Carbonization of Poultry Litter under Different Treatment Conditions. *ACS Sustain. Chem. Eng.* **2018**, *6*, 11265−11272.
(22) Obeid, R.; Lewis, D. M.; Smith, N.; Hall, T.; van Eyk, P. Reaction Kinetics and Characterization of Species in Renewable Crude from Hydrothermal Liquefaction of Mixtures of Polymer Compounds to Represent Organic Fractions of Biomass Feedstocks. *Energy Fuels* **2020**, *34*, 419−429.
(23) Posmanik, R.; Martinez, C. M.; Cantero-Tubilla, B.; Cantero, D. A.; Sills, D. L.; Cocero, M. J.; Tester, J. W. Acid and Alkali Catalyzed Hydrothermal Liquefaction of Dairy Manure Digestate and Food Waste. *ACS Sustain. Chem. Eng.* **2018**, *6*, 2724−2732.
(24) Sudibyo, H.; Pecchi, M.; Tester, J. W. Experimental-Based Mechanistic Study and Optimization of Hydrothermal Liquefaction of Anaerobic Digestates. *Sustain. Energy Fuels* **2022**, *6*, 2314−2329.
(25) Chen, Y.; Dong, L.; Miao, J.; Wang, J.; Zhu, C.; Xu, Y.; Chen, G. Y.; Liu, J. Hydrothermal Liquefaction of Corn Straw with Mixed Catalysts for the Production of Bio-Oil and Aromatic Compounds. *Bioresour. Technol.* **2019**, *294*, 122148.
(26) Davidson, S. D.; Lopez-Ruiz, J. A.; Zhu, Y.; Cooper, A. R.; Albrecht, K. O.; Dagle, R. A. Strategies to Valorize the Hydrothermal Liquefaction-Derived Aqueous Phase into Fuels and Chemicals. *ACS Sustain. Chem. Eng.* **2019**, *7*, 19889−19901.
(27) Yang, J.; He, Q.; Yang, L. A Review on Hydrothermal Co-Liquefaction of Biomass. *Appl. Energy* **2019**, *250*, 926−945.

(28) Schutyser, W.; Renders, T.; Van den Bosch, S.; Koelewijn, S. F.; Beckham, G. T.; Sels, B. F. Chemicals from Lignin: An Interplay of Lignocellulose Fractionation, Depolymerisation, and Upgrading. *Chem. Soc. Rev.* **2018**, *47*, 852−908.
(29) Sudibyo, H.; Pecchi, M.; Harwood, H.; Khare, M.; Karunwi, S.; Tan, G.; Tester, J. W. Thermodynamics and Kinetics of Struvite Crystallization from Hydrothermal Liquefaction Aqueous-Phase Considering Hydroxyapatite and Organics Coprecipitation. *Ind. Eng. Chem. Res.* **2022**, *61*, 6894−6908.
(30) Costamagna, P.; Giordano, A.; Lazzarini, Y.; Delucchi, M.; Busca, G. Process of Ammonia Removal from Anaerobic Digestion and Associated Ammonium Sulphate Production: Pilot Plant Demonstration. *J. Environ. Manage.* **2020**, *259*, 109841.
(31) Rao, U.; Posmanik, R.; Hatch, L. E.; Tester, J. W.; Walker, S. L.; Barsanti, K. C.; Jassby, D. Coupling Hydrothermal Liquefaction and Membrane Distillation to Treat Anaerobic Digestate from Food and Dairy Farm Waste. *Bioresour. Technol.* **2018**, *267*, 408−415.
(32) Sudibyo, H.; Wang, K.; Tester, J. W. Hydrothermal Liquefaction of Acid Whey: Effect of Feedstock Properties and Process Conditions on Energy and Nutrient Recovery. *ACS Sustain. Chem. Eng.* **2021**, *9*, 11403−11415.
(33) Matayeva, A.; Rasmussen, S. R.; Biller, P. Distribution of Nutrients and Phosphorus Recovery in Hydrothermal Liquefaction of Waste Streams. *Biomass Bioenergy* **2022**, *156*, 106323.
(34) Sudibyo, H.; Pecchi, M.; Harwood, H.; Khare, M.; Karunwi, S.; Tan, G.; Tester, J. W. Thermodynamics and Kinetics of Struvite Crystallization from Hydrothermal Liquefaction Aqueous-Phase Considering Hydroxyapatite and Organics Coprecipitation. *Ind. Eng. Chem. Res.* **2022**, *61*, 6894−6908.
(35) Wang, K.; Ma, Q.; Burns, M.; Sudibyo, H.; Sills, D. L.; Goldfarb, J. L.; Tester, J. W. Impact of Feed Injection and Batch Processing Methods in Hydrothermal Liquefaction. *J. Supercrit. Fluids* **2020**, *164*, 104887.
(36) American Society for Testing and Materials. *ASTM D5373-21 Standard Test Methods for Determination of Carbon, Hydrogen and Nitrogen in Analysis Samples of Coal and Carbon in Analysis Samples of Coal and Coke*: West Conshohocken, PA, United States, 2021.
(37) American Society for Testing and Materials. *ASTM D1426-15 Standard Test Methods for Ammonia Nitrogen in Water*: United States, 2015.
(38) American Public Health Association. *Standard Methods for the Examination of Water and Wastewater*, 23rd ed.; Clesceri, L., Greenberg, A., Eaton, A., Eds.; *APHA (American Public Health Association)*: Washington D.C., 2017.
(39) Crane, K. S.; Webb, B. L.; Allen, P. S.; Jolley, V. D. A Rapid Turbidimetric Potassium Test Modified for Use with the Pressurized Hot-Water Extraction. *Commun. Soil Sci. Plant Anal.* **2005**, *36*, 2687−2697.
(40) WELLS, R. W. Determination of Serum Calcium by Turbidimetry. *Am. J. Clin. Pathol.* **1948**, *18*, 576−578.
(41) Ryan, M. F.; Barbour, H. Magnesium Measurement in Routine Clinical Practice. *Ann. Clin. Biochem.* **1998**, *35*, 449−459.
(42) Channiwala, S. A.; Parikh, P. P. A Unified Correlation for Estimating HHV of Solid, Liquid and Gaseous Fuels. *Fuel* **2002**, *81*, 1051−1063.
(43) American Society for Testing and Materials. *ASTM E1131-20 Standard Test Method for Compositional Analysis by Thermogravimetry*: West Conshohocken, Pennsylvania, 2015; Vol. *08*.
(44) Zhang, H.; Wang, W.; Yuan, L.; Wei, Z.; Zhang, H.; Zhang, W. Quantitative Phase Analysis of Ti-3Al-5Mo-4.5 V Dual Phase Titanium Alloy by XRD Whole Pattern Fitting Method. *Mater. Charact.* **2022**, *187*, 111854.
(45) Gates-Rector, S.; Blanton, T. The Powder Diffraction File: A Quality Materials Characterization Database. *Powder Diffr.* **2019**, *34*, 352−360.
(46) Costa, N. R.; Lourenço, J.; Pereira, Z. L. Desirability Function Approach: A Review and Performance Evaluation in Adverse Conditions. *Chemom. Intell. Lab. Syst.* **2011**, *107*, 234−244.
(47) Nunes, V. O.; Fraga, A. C.; Silva, R. V. S.; Pontes, N. S.; Pinho, A. R.; Sousa-Aguiar, E. F.; Azevedo, D. A. Chemical Characterisation of Sugarcane Bagasse Bio-Oils from Hydrothermal Liquefaction: Effect of Reaction Conditions on Products Distribution and Composition. *J. Environ. Chem. Eng.* **2021**, *9*, 106513.
(48) Srokol, Z.; Bouche, A. G.; van Estrik, A.; Strik, R. C. J.; Maschmeyer, T.; Peters, J. A. Hydrothermal Upgrading of Biomass to Biofuel; Studies on Some Monosaccharide Model Compounds. *Carbohydr. Res.* **2004**, *339*, 1717−1726.
(49) Shen, T.; Hu, R.; Zhu, C.; Li, M.; Zhuang, W.; Tang, C.; Ying, H. Production of Cyclopentanone from Furfural over Ru/C with Al11.6PO23.7 and Application in the Synthesis of Diesel Range Alkanes. *RSC Adv.* **2018**, *8*, 37993−38001.
(50) Al-Hammadi, S.; da Silva, G. Thermal Decomposition and Isomerization of Furfural and 2-Pyrone: A Theoretical Kinetic Study. *Phys. Chem. Chem. Phys.* **2021**, *23*, 2046−2054.
(51) Zantioti-Chatzouda, E.-M.; Kotzabasaki, V.; Stratakis, M. Synthesis of γ-Pyrones and N -Methyl-4-Pyridones via the Au Nanoparticle-Catalyzed Cyclization of Skipped Diynones in the Presence of Water or Aqueous Methylamine. *J. Org. Chem.* **2022**, *87*, 8525−8533.
(52) Tan-Soetedjo, J. N. M.; van de Bovenkamp, H. H.; Abdilla, R. M.; Rasrendra, C. B.; van Ginkel, J.; Heeres, H. J. Experimental and Kinetic Modeling Studies on the Conversion of Sucrose to Levulinic Acid and 5-Hydroxymethylfurfural Using Sulfuric Acid in Water. *Ind. Eng. Chem. Res.* **2017**, *56*, 13228−13239.
(53) Sturgeon, M. R.; Kim, S.; Lawrence, K.; Paton, R. S.; Chmely, S. C.; Nimlos, M.; Foust, T. D.; Beckham, G. T. A Mechanistic Investigation of Acid-Catalyzed Cleavage of Aryl-Ether Linkages: Implications for Lignin Depolymerization in Acidic Environments. *ACS Sustain. Chem. Eng.* **2014**, *2*, 472−485.
(54) Wu, Z.; Hu, L.; Jiang, Y.; Wang, X.; Xu, J.; Wang, Q.; Jiang, S. Recent Advances in the Acid-Catalyzed Conversion of Lignin. *Biomass Convers. Biorefin.* **2020**, *13*, 519−539.
(55) Wang, Z.; Qin, H. Regioselective Synthesis of 1,2,3-Triazole Derivatives via 1,3-Dipolar Cycloaddition Reactions in Water. *Chem. Commun.* **2003**, *2*, 2450−2451.
(56) Bagchi, S.; Monga, A.; Kumar, S.; Deeksha, D.; Sharma, A. DABCO-Catalysed One-Pot Eco-Friendly Synthetic Strategies for Accessing Pyranochromenone and Bis(Benzochromenone) Compounds. *ChemistrySelect* **2018**, *3*, 12830−12835.
(57) Bugosen, S.; Mantilla, I. D.; Tarazona-Vasquez, F. Techno-Economic Analysis of Aniline Production via Amination of Phenol. *Heliyon* **2020**, *6*, No. e05778.
(58) Singh, R.; Veeramani, K.; Bajpai, R.; Kumar, A. High-Throughput Template-Free Continuous Flow Synthesis of Polyaniline Nanofibers. *Ind. Eng. Chem. Res.* **2019**, *58*, 5864−5872.
(59) Briand, M.; Haarlemmer, G.; Roubaud, A.; Fongarland, P. Evaluation of the Heat Produced by the Hydrothermal Liquefaction of Wet Food Processing Residues and Model Compounds. *ChemEngineering* **2022**, *6*, 2.
(60) Dong, L.; Lin, L.; Han, X.; Si, X.; Liu, X.; Guo, Y.; Lu, F.; Rudić, S.; Parker, S. F.; Yang, S.; Wang, Y. Breaking the Limit of Lignin Monomer Production via Cleavage of Interunit Carbon−Carbon Linkages. *Chem* **2019**, *5*, 1521−1536.
(61) Hardacre, C.; Nancarrow, P.; Rooney, D. W.; Thompson, J. M. Friedel-Crafts Benzoylation of Anisole in Ionic Liquids: Catalysis, Separation, and Recycle Studies. *Org. Process Res. Dev.* **2008**, *12*, 1156−1163.
(62) Arceo, E.; Ellman, J. A.; Bergman, R. G. A Direct, Biomass-Based Synthesis of Benzoic Acid: Formic Acid-Mediated Deoxygenation of the Glucose-Derived Materials Quinic Acid and Shikimic Acid. *ChemSusChem* **2010**, *3*, 811−813.
(63) Cirillo, P. F.; Caccavale, A.; DeLuna, A. Green Fischer Indole Synthesis Using a Steroidal Ketone in a Conductively Heated Sealed-Vessel Reactor for the Advanced Undergraduate Laboratory. *J. Chem. Educ.* **2021**, *98*, 567−571.

https://doi.org/10.1021/acs.energyfuels.2c03860
Energy Fuels XXXX, XXX, XXX−XXX

(64) Amarnath, V.; Anthony, D. C.; Amarnath, K.; Valentine, W. M.; Wetterau, L. A.; Graham, D. G. Intermediates in the Paal-Knorr Synthesis of Pyrroles. *J. Org. Chem.* **1991**, *56*, 6924−6931.
(65) Gati, W.; Rammah, M. M.; Rammah, M. B.; Couty, F.; Evano, G. De Novo Synthesis of 1,4-Dihydropyridines and Pyridines. *J. Am. Chem. Soc.* **2012**, *134*, 9078−9081.
(66) Park, J.; Kim, D. H.; Das, T.; Cho, C. G. Intramolecular Fischer Indole Synthesis for the Direct Synthesis of 3,4-Fused Tricyclic Indole and Application to the Total Synthesis of (-)-Aurantioclavine. *Org. Lett.* **2016**, *18*, 5098−5101.
(67) Dadashipour, M.; Ishida, Y.; Yamamoto, K.; Asano, Y. Discovery and Molecular and Biocatalytic Properties of Hydroxynitrile Lyase from an Invasive Millipede, Chamberlinius Hualienensis. *Proc. Natl. Acad. Sci. U.S.A.* **2015**, *112*, 10605−10610.
(68) Sudibyo, H.; Tester, J. W. Probing Elemental Speciation in Hydrochar Produced from Hydrothermal Liquefaction of Anaerobic Digestates Using Quantitative X-Ray Diffraction. *Sustain. Energy Fuels* **2022**, *6*, 5474−5490.
(69) Lu, J.; Li, H.; Zhang, Y.; Liu, Z. Nitrogen Migration and Transformation during Hydrothermal Liquefaction of Livestock Manures. *ACS Sustain. Chem. Eng.* **2018**, *6*, 13570−13578.
(70) Naredla, R. R.; Klumpp, D. A. Benzamide Synthesis by Direct Electrophilic Aromatic Substitution with Cyanoguanidine. *Tetrahedron Lett.* **2012**, *53*, 4779−4781.
(71) Montagne, C.; Shiers, J. J.; Shipman, M. Rapid Generation of Molecular Complexity Using "sequenced" Multi-Component Reactions: One-Pot Synthesis of 5,5′-Disubstituted Hydantoins from Methyleneaziridines. *Tetrahedron Lett.* **2006**, *47*, 9207−9209.
(72) Tikhov, R. M.; Kuznetsov, N. Y. Construction of Piperidine-2,4-Dione-Type Azaheterocycles and Their Application in Modern Drug Development and Natural Product Synthesis. *Org. Biomol. Chem.* **2020**, *18*, 2793−2812.
(73) Prado, G. H. C.; Rao, Y.; de Klerk, A. Nitrogen Removal from Oil: A Review. *Energy Fuels* **2017**, *31*, 14−36.
(74) Chaka, A. M. Ab Initio Thermodynamics of Hydrated Calcium Carbonates and Calcium Analogues of Magnesium Carbonates: Implications for Carbonate Crystallization Pathways. *ACS Earth Space Chem.* **2018**, *2*, 210−224.
(75) Tone, T.; Koga, N. Thermally Induced Aragonite-Calcite Transformation in Freshwater Pearl: A Mutual Relation with the Thermal Dehydration of Included Water. *ACS Omega* **2021**, *6*, 13904−13914.
(76) Boanini, E.; Silingardi, F.; Gazzano, M.; Bigi, A. Synthesis and Hydrolysis of Brushite (DCPD): The Role of Ionic Substitution. *Cryst. Growth Des.* **2021**, *21*, 1689−1697.
(77) Hodge, C. A.; Motes, T. W. Production of High-Quality Liquid Fertilizers from Wet-Process Acid via Urea Phosphate. *Fertil. Res.* **1994**, *39*, 59−69.
(78) Li, Y.; Hua, D.; Xu, H.; Jin, F.; Zhao, Y.; Chen, L.; Zhao, B.; Rosendahl, L. A.; Zhu, Z. Energy Recovery from High Ash-Containing Sewage Sludge: Focusing on Performance Evaluation of Bio-Fuel Production. *Sci. Total Environ.* **2022**, *843*, 157083.
(79) Leng, L.; Yang, L.; Leng, S.; Zhang, W.; Zhou, Y.; Peng, H.; Li, H.; Hu, Y.; Jiang, S.; Li, H. A Review on Nitrogen Transformation in Hydrochar during Hydrothermal Carbonization of Biomass Containing Nitrogen. *Sci. Total Environ.* **2021**, *756*, 143679.
(80) Bockisch, C.; Lorance, E. D.; Hartnett, H. E.; Shock, E. L.; Gould, I. R. Kinetics and Mechanisms of Dehydration of Secondary Alcohols under Hydrothermal Conditions. *ACS Earth Space Chem.* **2018**, *2*, 821−832.
(81) Mahadevan Subramanya, S.; Savage, P. E. Identifying and Modeling Interactions between Biomass Components during Hydrothermal Liquefaction in Sub-, Near-, and Supercritical Water. *ACS Sustain. Chem. Eng.* **2021**, *9*, 13874−13882.
(82) Ghavami, N.; Özdenkçi, K.; Salierno, G.; Björklund-Sänkiaho, M.; De Blasio, C. Analysis of Operational Issues in Hydrothermal Liquefaction and Supercritical Water Gasification Processes: A Review. *Biomass Convers. Biorefin.* **2021**, 1−28.
(83) Zhai, Z.; Li, X.; Tang, C.; Peng, J.; Jiang, N.; Bai, W.; Gao, H.; Liao, Y. Decarbonylation of Lactic Acid to Acetaldehyde over Aluminum Sulfate Catalyst. *Ind. Eng. Chem. Res.* **2014**, *53*, 10318−10327.

https://doi.org/10.1021/acs.energyfuels.2c03860
Energy Fuels XXXX, XXX, XXX−XXX